INTERFEROMETRIC DETECTION OF GRAVITATIONAL WAVES

Adalberto GIAZOTTO

Istituto Nazionale di Fisica Nucleare, Sezione di Pisa, Via Vecchia Livornese 582/a, 56010 S. Piero a Grado, Pisa, Italy

INTERFEROMETRIC DETECTION OF GRAVITATIONAL WAVES

Adalberto GIAZOTTO

Istituto Nazionale di Fisica Nucleare, Sezione di Pisa, Via Vecchia Livornese 582/a, 56010 S. Piero a Grado, Pisa, Italy

Contents:

Abstract:

The theoretical and experimental methods involved in the interferometric detection of gravitational waves are reviewed and an attempt of historical analysis is given. The delay line and Fabry–Pérot techniques for storing light in the interferometer are analyzed together with the types of noise competing with the gravitational wave signal.

Introduction

This Report has not been conceived for specialist readers but for those who are interested in the techniques and the calculation methods involved in the project of interferometric antennas for gravitational wave (GW) detection. I think that my contribution to this didactical approach is more useful than to make a repetition of the already excellent review articles on the field of GW generation and detection [Braginskii and Rudenko 1978, Douglass and Braginskii 1979, Weiss 1979, Thorne 1980, 1987, Hough et al. 1987]. On the other hand, daily contact with the problems arising from the technical solutions necessary to plan the very large interferometer VIRGO gave me the push to write this Report; I realize that regretfully many authors will not be quoted in the text, as will be some experimental results. I apologize for such omissions.

The generation of laboratory GWs with the purpose of detecting them in a "Hertz experiment" [Misner, Thorne and Wheeler 1973 (MTW), Braginskii and Manoukine 1974, Douglass and Braginskii 1979] is unfortunately an almost hopeless enterprise. Extremely high-energy particles accelerated in the next generation accelerators have been considered as potential candidates for the "laboratory" generation of GWs [Braginskii et al. 1977, Vinet 1981, Diambrini, Palazzi and Fargion 1987], but even in this case many more years will be needed to succeed. Astrophysical sources seem to be nowadays the only possible emitters of detectable gravitational radiation; in the following I will mention briefly the best candidate sources likely to be detected in the coming years.

The amplitude of the GWs emitted will be denoted by means of the dimensionless quantity (see section 1)

$$h_{\alpha\beta}^{TT} \simeq \frac{2G}{c^4 R_0} \frac{d^2}{dt^2} \int \rho(3x^\alpha x^\beta - \delta_{\alpha\beta}x^2)\,dv \;, \tag{I.1}$$

where G is the Newton constant, c the light speed, R_0 the distance from the source, ρ the source mass distribution and the integral is calculated over the source volume. The effect it produces on the separation L of two freely falling masses (see section 2) is a variation $\Delta L_\alpha \sim \frac{1}{2}L^\beta h_{\alpha\beta}^{TT}$, which is a measurable quantity. Hence I will denote by $h = h_{\alpha\beta}^{TT}$ the strength of the sources.

Historically the most discussed and most likely producer of detectable GWs has been the collapse of a star. In this process the matter explosion, due to eq. (I.1), must not be of spherical shape for the emission of GW; an approximate formula is

$$h \simeq 5 \times 10^{-21} \left(\frac{\eta}{10^{-2}}\right)^{1/2} \left(\frac{15\,\text{Mpc}}{R_0}\right) \left(\frac{1\,\text{kHz}}{\nu}\right) \left(\frac{10^{-3}\,\text{s}}{\tau}\right)^{1/2} \;, \tag{I.2}$$

where $\eta = \Delta E/M_0 c^2$ is the fraction of energy emitted in GWs, R_0 the distance, ν the observation frequency and $\tau \simeq d_s/c$ the time it takes the collapse shock to traverse the source dimension d_s. The quantity η is the fraction of total energy converted in GW, supposed to be <0.2. The explosion rate is expected to be 1 in 40 years in the galaxy and a few per year in the Virgo cluster. The pulse duration τ is usually considered to be $\simeq 1$ ms, hence detectors are tuned accordingly.

Other classes of events, of far less certain predictability, are those involving black holes. The infall of a particle strongly produces GWs; moreover, if the particle spirals into the black hole, the radiation is 100 times more intense than for radial infall [Kojima and Nakamusa 1984].

A mechanism surely emitting high-intensity GWs is the rotation of compact binary objects such as

neutron stars; since the star diameter can be $\simeq 10$ km, the mutual distance can be so small that before coalescence very intense radiation is produced. The signal amplitude is

$$h \simeq 10^{-23}\left(\frac{100\,\mathrm{Mpc}}{R_0}\right)\left(\frac{M}{M_0}\right)^{2/3}\left(\frac{\mu}{M_0}\right)\left(\frac{\nu}{100\,\mathrm{Hz}}\right)^{2/3}, \tag{I.3}$$

where M and μ are the total and reduced mass, respectively, and M_0 the solar mass. The time elapsed around the frequency ν is

$$t \simeq 7.8\left(\frac{100}{\nu}\right)^{8/3}\left(\frac{M_0}{M}\right)^{2/3}\left(\frac{M_0}{\mu}\right)\,\mathrm{s}. \tag{I.4}$$

Since the detector S/N ratio is proportional to $t^{1/2}$, it follows from (I.4) and (I.3) that the S/N ratio increases as $\nu^{-2/3}$, i.e., detectors having an extended bandwidth at low frequency are more likely to detect these sources. An estimate of Clark et al. [1979] gives $\simeq 3$ events per year in a sphere of 100 Mpc radius.

Pulsars have been interpreted as rotating neutron stars having an off-axis magnetic dipole field [Pacini 1968, Gold 1968], and are considered to be the best candidates as continuous GW emitters. A surface protuberance or aspherical shape with an ellipticity ε could give an amplitude [Zimmermann and Szedenits 1979, Zimmermann 1980]

$$h \simeq 10^{-23}\varepsilon\left(\frac{\nu}{10\,\mathrm{Hz}}\right)^2\left(\frac{10\,\mathrm{kpc}}{R_0}\right), \tag{I.5}$$

where ν is the GW frequency, twice the rotation frequency because of eq. (I.1). Upper limits to the GW emission from the Vela and Crab pulsars have been estimated by Zimmermann [1978] to be $h \simeq 3 \times 10^{-24}$ and 2×10^{-26} (standard Crab model), respectively, but according to the model of Pandharipande et al. [1976], the Crab pulsar may have an amplitude upper limit of $h \simeq 10^{-25}$.

Since the total number of pulsars in the Galaxy has been estimated to be $\sim 10^5$ [Taylor and Manchester 1977, Lyne et al. 1985] and the fraction of pulsars with GW frequency >10 Hz is about 5% [Manchester and Taylor 1981, Rawley et al. 1986, Barone et al. 1988] we can expect several thousand pulsars having GW frequency $\nu > 10$ Hz and in the frequency range of the kilometric interferometric detectors.

The Heisenberg uncertainty principle sets a fundamental limit to the strain sensitivity measured by means of two freely falling masses M separated by a distance L, in a time $\bar{T}$,

$$h \simeq \frac{1}{\Omega L}\sqrt{\frac{2\hbar}{M\bar{T}}} \simeq 1.5 \times 10^{-25}\left(\frac{10^3\,\mathrm{m}}{L}\right)\left(\frac{1\,\mathrm{Hz}}{\nu}\right)\left(\frac{10^7\,\mathrm{s}}{\bar{T}}\right)^{1/2}\left(\frac{10^2\,\mathrm{kg}}{M}\right)^{1/2}, \tag{I.6}$$

where $\Omega = 2\pi\nu$ and $\hbar$ is the reduced Planck constant. With $M = 300$ kg, $\bar{T} = 3 \times 10^7$ s, $L = 3 \times 10^3$ m, at the Crab frequency ($\nu = 60$ Hz) eq. (I.6) gives $h > 1.5 \times 10^{-28}$.

If a pulsar and a star form a binary system there may be a drainage of star matter from the pulsar's surface due to the high gravitational field. This matter is accreting around the neutron star, which is then spun up; the accretion may then reach the Chandrasekhar [1970]–Friedman–Schutz [1978] instability point and strongly emit GWs with an expected amplitude [Wagoner 1984]

$$h \simeq 2 \times 10^{-28} \left(\frac{300 \, \text{Hz}}{\nu} \right) \left(\frac{F_x}{10^{-17} \, \text{J/cm}^2 \, \text{s}} \right)^{1/2} , \tag{I.7}$$

where F_x is the flux of the emitted X-rays.

The stochastic background of GWs produced by all sources has an expected amplitude (for a review see Hough et al. [1986], Thorne [1987])

$$h \simeq 6 \times 10^{-26} \left(\frac{\Omega_{\text{GW}}}{10^{-10}} \right)^{1/2} \left(\frac{100 \, \text{Hz}}{\nu} \right) , \tag{I.8}$$

where Ω_{GW} is the ratio of the source energy density in a bandwidth ν to that necessary to close the universe $(10^{-15} \, \text{J/cm}^3)$.

The basic and, to my opinion, the first idea of the interferometric detection of GWs is, clearly stated, contained in a paper of Gertsenshtein and Pustovoit [1963]; their idea is that ". . . . it should be possible to detect gravitational waves by the shift of the bands in an optical interferometer". The first complete work on the noise competing with the GW signal in an interferometric antenna is due to Weiss [1972]; it is also his merit to have advanced the idea of using a "stable" cavity such as the Herriot [1964] delay line, and fast light phase modulation to get rid of the laser's amplitude fluctuations. But the very first experimental attempt, giving high sensitivity in the measurement of the test mass displacement is due to Forward [1978]. Forward used retroflectors to reflect the beam back to a beam splitter and used active controls to lock the interferometer to a fringe; he obtained a spectral strain sensitivity of $\tilde{h} > 2 \times 10^{-16} \, \text{Hz}^{-1/2}$ for $\nu > 2 \, \text{kHz}$. The Max Planck at Munich group [Billing et al. 1979], following Weiss' delay lines idea, carried out the construction of a 30 m interferometer having a sensitivity $\tilde{h} \simeq 8 \times 10^{-20} \, \text{Hz}^{-1/2}$.

The alternative to using delay lines is using Fabry–Pérot cavities; this scheme, which was pursued by Drever [Drever et al. 1980, 1981], is very elegant even though it requires more sophisticated optical and feed back design than in the delay line case. Two Fabry–Pérot interferometers are now working in Glasgow and Caltech with a sensitivity $\tilde{h} \simeq 1.2 \times 10^{-19} \, \text{Hz}^{-1/2}$ [Ward et al. 1987] and $\tilde{h} \simeq 5 \times 10^{-19} \, \text{Hz}^{-1/2}$ [Spero 1986], respectively.

Several optical schemes have been invented for increasing the interferometer's sensitivity: light power recycling [Drever 1982] allows the reuse of the unused light from the interferometer; the synchronous recycling scheme [Ruggiero 1979, Drever 1981] allows an increase in the interferometer's sensitivity to periodic signals as do the methods of detuned recycling [Vinet et al. 1988] and dual recycling [Meers 1988]. Of all these schemes only that of power recycling has been tested experimentally [Rüdiger et al. 1987, Man et al. 1987] with success. All the signal recycling schemes will be tested, perhaps painfully, in the future kilometric interferometers.

Another approach to increasing the sensitivity has been given by Caves [1980], who was the first to realize that photon number fluctuations in the interferometer's arms could be produced by vacuum fluctuations of the light field at the unused port of the beam splitter; the idea was to inject into this port a squeezed photon state, i.e. a state having phase fluctuations smaller than Poissonian but with larger amplitude fluctuations. The existence of these states has been demonstrated experimentally and this has led the Munich group [Gea-Banacloche and Leuchs 1987] to experimentally explore the sqeezing route.

At this very moment (February 1989) it seems that there is a likely chance that the construction of four large interferometers will be approved: the German–Scottish one, the French–Italian one and the two American ones. Japan and Australia are likely to join this group. The need of several large

interferometers is also dictated by the necessity of making coincidence detection of GW signals.

There is also a finite chance that GWs will be discovered meanwhile by the bar detectors and this will finally convince physicists from other fields to join what I consider the most exciting and, at the same time, frustrating experience a physicist can have.

This Report has been subdivided into 14 sections: in section 1 the generation mechanism of GWs and in section 2 the interaction of GWs with matter are described. Delay lines and Fabry–Pérot optical interferometers are described in sections 3 and 4, respectively. The recycling schemes are described in section 5, the laser intensity noise in section 6 and the noise due to the laser linewidth in section 7. The laser lateral beam jitter noise is described in section 8 and the noise due to gas pressure fluctuations in section 9. The thermal noise is described in section 10, the seismic noise in section 11, the radiation pressure effects in section 12, the cosmic ray background in section 13 and finally, a pictorial description of source intensities and relevant noises is presented in section 14.

1. The generation of gravitational waves and the transverse traceless gauge

In Einstein's Theory of General Relativity (TGR) [Einstein 1916] Gravitational Waves (GWs) are shown to be ripples in the space–time curvature propagating with the speed of light. Under the hypothesis of weak fields a perturbation $h_{\mu\nu}$ to the flat metric tensor

$$\eta_{\mu\nu} = \begin{pmatrix} 1 & 0 & 0 & 0 \\ 0 & -1 & 0 & 0 \\ 0 & 0 & -1 & 0 \\ 0 & 0 & 0 & -1 \end{pmatrix} \tag{1.1}$$

is created by the energy–momentum tensor τ_{ik} according to the equation (see MTW)

$$\Box \Psi_{ik} = (8\pi G/c^4)\tau_{ik} , \tag{1.2}$$

where $\Psi_{ik} = h_{ik} - \frac{1}{2}\delta_{ik}h_\mu^\mu$, G is the Newton constant and c the speed of light. From momentum–energy conservation,

$$\partial_\mu \tau_{\mu\nu} = 0 , \tag{1.3}$$

and considering that $\tau_{00} = \rho c^2$, where ρ is the matter density, it follows that [Landau and Lifshitz 1951]

$$\Psi_{\alpha\beta} = -\frac{2G}{c^4 R_0}\left(\frac{\partial^2}{\partial t^2}\int \rho x^\alpha x^\beta \, d\nu\right)_{t-R_0/c} , \tag{1.4}$$

where R_0 is the distance from the source; eq. (1.4) is valid when the matter speed is far less than c and when the GW wavelength is much larger than the source dimensions. From eq. (1.4) it follows that the GW field is produced by the second moment of the mass distribution.

Since Ψ_μ is a symmetric tensor it has 10 independent elements, which are reduced to 6 since eq. (1.3) gives

$$\partial_\mu \Psi_{\mu\nu} = 0 . \tag{1.5}$$

The number of independent elements of $\Psi_{\mu\nu}$ can be further reduced by applying the coordinate transformation

$$x'_\mu = x_\mu + \varepsilon_\mu \,, \tag{1.6}$$

where ε_μ are infinitesimal functions which must leave unchanged the line element

$$ds^2 = g_{\mu\nu}\, dx^\mu\, dx^\nu \,. \tag{1.7}$$

Equation (1.7) imposes

$$\Box \varepsilon_\mu = 0 \,, \tag{1.8}$$

$$h'_{\mu\nu} = h_{\mu\nu} - \partial\varepsilon_\mu/\partial x_\nu - \partial\varepsilon_\nu/\partial x_\mu \,. \tag{1.9}$$

Hence writing Ψ_{ik} as a plane wave propagating in the k direction at speed c,

$$\Psi_{ik} = A_{ik}\, e^{ik_r x^r} \,, \qquad k^r k_r = 0 \,, \tag{1.10}$$

and putting [see eq. (1.9)]

$$\varepsilon_\mu = C_\mu\, e^{ik_r x^r} \,, \tag{1.11}$$

we can define a four-velocity V^k and choose C_μ such as to give

$$A_{ik} V^k = 0 \,. \tag{1.12}$$

But these four equations are not independent since $k^i A_{ik} V^k = 0$ for any given k; hence a further condition can be applied and we impose

$$A^\mu_\mu = 0 \,. \tag{1.13}$$

This condition gives $h^\mu_\mu = 0$ and

$$\Psi_{\mu\nu} = h_{\mu\nu} \,. \tag{1.14}$$

Equations (1.5), (1.12) and (1.13) define the Transverse Traceless (TT) gauge (see MTW); by choosing $V^0 = 1$, $V = 0$ we obtain

$$h^{TT}_{\mu 0} = 0 \,, \quad \text{i.e. only spatial components} \neq 0 \,,$$

$$h^{TT}_{KJ,J} = 0 \,, \quad \text{i.e. divergence-free spatial components} \,, \tag{1.15}$$

$$h^{TT}_{KK} = 0 \,, \quad \text{traceless} \,.$$

Let us assume the wave propagates along the x_3 axis; then

$$k = (k, 0, 0, k),$$
(1.16)

and from eq. (1.15) it follows that

$$h_{3K}^{TT} = 0, \qquad h_{11}^{TT} = -h_{22}^{TT} = 0, \qquad h_{12}^{TT} = h_{21}^{TT}.$$
(1.17)

In matrix form

$$h_{ik}^{TT} = \begin{pmatrix} 0 & 0 & 0 & 0 \\ 0 & h_{11}^{TT} & h_{12}^{TT} & 0 \\ 0 & h_{12}^{TT} & -h_{11}^{TT} & 0 \\ 0 & 0 & 0 & 0 \end{pmatrix} = h_{11}^{TT} \begin{pmatrix} 0 & 0 & 0 & 0 \\ 0 & 1 & 0 & 0 \\ 0 & 0 & -1 & 0 \\ 0 & 0 & 0 & 0 \end{pmatrix} + h_{12}^{TT} \begin{pmatrix} 0 & 0 & 0 & 0 \\ 0 & 0 & 1 & 0 \\ 0 & 1 & 0 & 0 \\ 0 & 0 & 0 & 0 \end{pmatrix} = A_+ e_{ik}^+ + A_\times e_{ik}^\times.$$
(1.18)

The two polarizations e_{ik}^+ and $e_{ik}^\times$ are exchanged by a rotation R of $\pi/4$ around the x_3 axis, i.e.,

$$R(\pi/4) = \frac{1}{\sqrt{2}} \begin{pmatrix} 0 & 0 & 0 & 0 \\ 0 & 1 & 1 & 0 \\ 0 & -1 & 1 & 0 \\ 0 & 0 & 0 & 0 \end{pmatrix},$$

$$R(\pi/4) e^+ R^{-1}(\pi/4) = -e^\times, \qquad R(\pi/4) e^\times R^{-1}(\pi/4) = e^+.$$
(1.19)

This behaviour under rotation is proper to a spin-2 field.
The Riemann tensor

$$R_{iklm} = \frac{1}{2} \left(\frac{\partial^2 h_{im}}{\partial x^k \partial x^l} + \frac{\partial^2 h_{kl}}{\partial x^i \partial x^m} - \frac{\partial^2 h_{km}}{\partial x^i \partial x^l} - \frac{\partial h_{il}^2}{\partial x^k \partial x^m} \right)$$
(1.20)

with the conditions of eq. (1.11) becomes simply

$$R_{iklm} \quad \Rightarrow \quad R_{0\alpha0\beta} = -\tfrac{1}{2} \ddot{h}_{\alpha\beta}^{TT}.$$
(1.21)

The TT part of eq. (1.4) can be evaluated by applying to $\Psi_{\alpha\beta}$ the TT projection operator (see MTW)

$$P_{jk} = \delta_{jk} - n_j n_k,$$
(1.22)

where n is the unit vector in the direction in which we want to evaluate the TT part of the GW amplitude; hence

$$\Psi_{\alpha\beta}^{TT} = P_{\alpha j} \Psi_{jl} P_{l\beta} - \tfrac{1}{2} P_{\alpha\beta} \Psi_{lm} P_{lm}.$$
(1.23)

It is easy to verify that from eqs. (1.23), (1.4) and (1.15) it follows that $\Psi_{\alpha\beta}^{TT} n_\beta = 0$, $\Psi_{\alpha\alpha}^{TT} = 0$, and

$$h_{\alpha\beta}^{TT} = -\frac{2G}{c^4 R_0} \left(\frac{\partial^2}{\partial t^2} \int \rho(P_{\alpha j} x^j x^l P_{l\beta} - \tfrac{1}{2} P_{\alpha\beta} x^l x^m P_{lm}) \, dv \right) = -\frac{2G}{c^4 R_0} \ddot{D}_{\alpha\beta}^{TT},$$
(1.24)

where $D_{\alpha\beta}$ is the reduced quadrupole momentum of the GW emitting mass system.

2. The detection of gravitational waves

A particle moving freely under the action of a gravitational force has its coordinates x^μ satisfying the geodesic equation

$$\frac{d^2 x^\mu}{d\tau^2} + \Gamma^\mu_{\nu\lambda} \frac{dk^\nu}{d\tau} \frac{dx^\lambda}{d\tau} = 0 \,, \tag{2.1}$$

where τ is proportional to the particle's proper time and

$$\Gamma^\mu_{\nu\lambda} = \tfrac{1}{2} g^{\mu m} \left(\frac{\partial g_{m\nu}}{\partial x^\lambda} + \frac{\partial g_{m\lambda}}{\partial x^\nu} - \frac{\partial g_{\nu\lambda}}{\partial x^m} \right) \tag{2.2}$$

are the Christoffel symbols. It is always possible to find a space–time trajectory in which $\Gamma^\mu_{\nu\lambda} = 0$ at any time; along this trajectory the particle is freely falling. It is easy to show that the separation ξ^α between two particles A and B satisfies the geodesic deviation equation

$$\frac{D^2 \xi^\alpha}{d\tau^2} + R^\alpha_{\beta\gamma\delta} \xi^\gamma \frac{dx^\beta}{d\tau} \frac{dx^\delta}{d\tau} = 0 \,, \tag{2.3}$$

where D^2 is the second covariant derivative,

$$\frac{D^2 \xi^\alpha}{d\tau^2} = \frac{d^2 \xi^\alpha}{d\tau^2} + \frac{d\Gamma^\alpha_{\beta\mu}}{d\tau} \xi^\beta \frac{dx^\mu}{d\tau} + \Gamma^\alpha_{\beta\mu} \frac{d}{d\tau} \left(\xi^\beta \frac{dx^\mu}{d\tau} \right) + \Gamma^\alpha_{\beta\mu} \left(\frac{d\xi^\beta}{d\tau} + \Gamma^\alpha_{\beta\mu} \xi^\beta \frac{dx^\mu}{d\tau} \right) \frac{dx^\mu}{d\tau} \,. \tag{2.4}$$

With the purpose of evaluating ξ^α let us put $x = 0$ in the center of mass system (CMS) of particle A (see MTW), the time x_0 equal to the proper time τ and the coordinate axis connected to gyroscopes carried by A. At $x = 0$, since A is freely falling along the geodesic line, we obtain

$$(\Gamma^\alpha_{\beta\gamma})_{x=0} = (d\Gamma^\alpha_{\beta\gamma}/d\tau)_{x=0} = 0 \,, \tag{2.5}$$

and eq. (2.2) becomes

$$D^2 \xi^\alpha / d\tau^2 = d^2 \xi^\alpha / d\tau^2 \,. \tag{2.6}$$

Introducing eqs. (1.21) and (2.6) into eq. (2.3) and considering that, to first order in $h^{\mathrm{TT}}_{\mu\nu}$, $t \cong \tau$, where t is the observation time, we obtain

$$d^2 \xi^\alpha / dt^2 = -R_{\alpha 0\beta 0} \xi^\beta = \tfrac{1}{2} (d^2/dt^2) h^{\mathrm{TT}}_{\alpha\beta} \xi^\beta \,. \tag{2.7}$$

From eq. (2.7) we can see the effects of GW polarization on the detector; if the GW is propagating along the z axis and the masses A and B are located as in fig. 2.1, then

$$\xi^\alpha = (x_{\mathrm{A}} - x_{\mathrm{B}})^\alpha \,. \tag{2.8}$$

Putting

$$F_\alpha = M \, d^2 \xi^\alpha / dt^2 = \tfrac{1}{2} M \, (d^2/dt^2) h^{\mathrm{TT}}_{\alpha\beta} \xi^\beta \,, \tag{2.9}$$
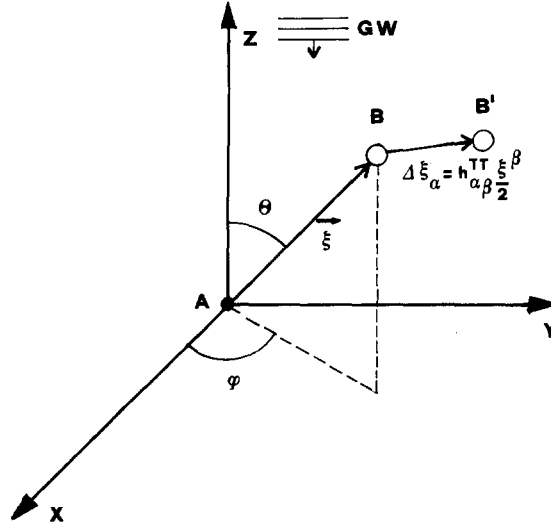
Fig. 2.1. In an inertial system having the origin in the center of mass of mass A the effect of a GW traveling along the z axis is to displace the mass B from the equilibrium position by an amount $\Delta \xi^\alpha = \frac{1}{2} h_{\alpha\beta}^{TT} \xi^\beta$ [see eq. (2.7)].

and considering that the only independent components of $h_{\alpha\beta}^{TT}$ are h_{11}^{TT} and h_{12}^{TT}, we can write the projection F of F_α along the line connecting A to B,

$$F(\theta, \varphi) = F_\alpha \xi^\alpha / |\xi| = \frac{1}{2} |\xi| M(\ddot{h}_{11}^{TT} \sin^2\theta \cos 2\varphi + \ddot{h}_{12}^{TT} \sin^2\theta \sin 2\varphi) .$$ (2.10)

In eq. (2.10) the tidal character of the force produced by a GW is clearly shown by the term $|\xi|$. It is also evident from eq. (2.10) that $F = 0$ if the mass separation ξ^α is in the GW propagation direction.

In the interferometric antenna the mirrors are attached to masses suspended with wires like pendula. With reference to fig. 2.2, the beam splitter in the origin has mass m_1 and the other two mirrors have mass m_2 and m_3, respectively, and are placed at a distance L from the origin; ξ_i are the coordinates of the masses m_i in the CMS. The CMS coordinates are

$$x_{cms} = Lm_3/(m_1 + m_2 + m_3) , \qquad y_{cms} = Lm_2/(m_1 + m_2 + m_3) .$$ (2.11)

For the sake of simplicity we assume that the GW is propagating along the z axis; under this condition, using eq. (2.7), the acceleration of the mirrors produced by the GW interaction becomes

$$(\ddot{x}_1)_{GW} = -\frac{1}{2}(\ddot{h}_{11}^{TT} x_{cms} + \ddot{h}_{12}^{TT} y_{cms}) , \qquad (\ddot{x}_3)_{GW} = -\frac{1}{2}[\ddot{h}_{11}^{TT}(L - x_{cms}) - \ddot{h}_{12}^{TT} y_{cms}] ,$$
$$(\ddot{y}_1)_{GW} = -\frac{1}{2}(\ddot{h}_{21}^{TT} x_{cms} + \ddot{h}_{22}^{TT} y_{cms}) , \qquad (\ddot{y}_2)_{GW} = \frac{1}{2}[-\ddot{h}_{21} x_{cms} + \ddot{h}_{22}^{TT}(L - y_{cms})] .$$ (2.12)

The equations of motion of the mirrors read

$$\ddot{x}_1 + \tau_1^{-1}(\dot{x}_1 - \dot{\bar{x}}_1) + (g/l_1)(x_1 - \bar{x}_1) = (\ddot{x}_1)_{GW} , \qquad \ddot{x}_3 + \tau_3^{-1}(\dot{x}_3 - \dot{\bar{x}}_3) + (g/l_3)(x_3 - \bar{x}_3) = (\ddot{x}_3)_{GW} ,$$
$$\ddot{y}_1 + \tau_1^{-1}(\dot{y}_1 - \dot{\bar{y}}_1) + (g/l_1)(y_1 - \bar{y}_1) = (\ddot{y}_3)_{GW} , \qquad \ddot{y}_2 + \tau_2^{-1}(\dot{y}_2 - \dot{\bar{y}}_2) + (g/l_2)(y_2 - \bar{y}_2) = (\ddot{y}_2)_{GW} ,$$ (2.13)
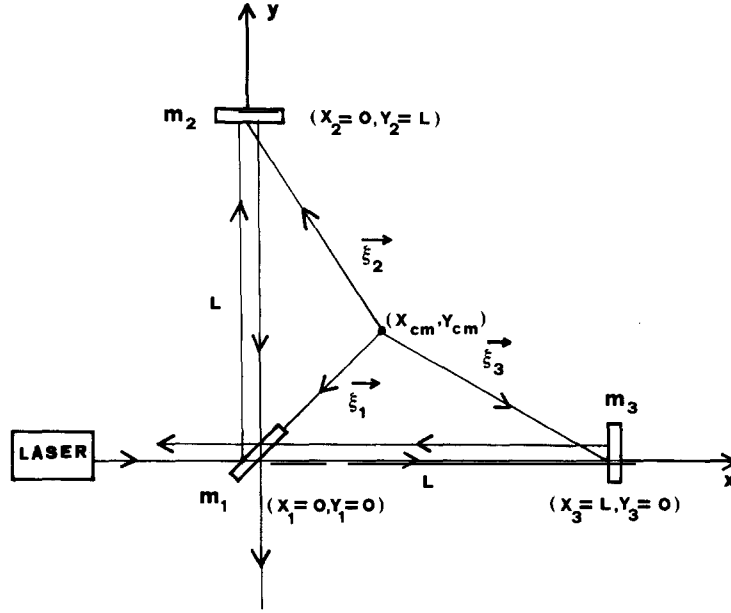
Fig. 2.2. The interferometer's mirrors, having mass m_1, m_2 and m_3, are located at (x, y) positions $(0,0)$, $(0, L)$ and $(L,0)$, respectively. The acceleration of the mirrors produced by a GW traveling along the z axis is calculated introducing their coordinates in the CMS, ξ_i, into eq. (2.9). The inertial reference system has the origin in the center of mass of the mirror system.

where τ_i and l_i are, respectively, the relaxation time and the length of the ith pendulum and $\bar{x}_i$, $\bar{y}_i$ are the pendulum suspension point displacements due to seismic noise. Equations (2.13) can be solved exactly, but for the sake of simplicity we assume $\tau_i = \tau_j$ and $l_i = l_j$; then we can subtract the first equation from the second and the third from the fourth, obtaining

$$\Delta\ddot{x} + \tau^{-1}(\Delta\dot{x} - \Delta\dot{\bar{x}}) + (\Delta x - \Delta\bar{x})\omega_0^2 = -\tfrac{1}{2}\ddot{h}_{11}^{TT}L\,, \quad \Delta\ddot{y} + \tau^{-1}(\Delta\dot{y} - \Delta\dot{\bar{y}}) + (\Delta y - \Delta\bar{y})\omega_0^2 = -\tfrac{1}{2}\ddot{h}_{22}^{TT}L\,,$$
$$(2.14)$$

where $\Delta x = x_1 - x_3$, $\Delta y = y_1 - y_2$, $\Delta\bar{x} = \bar{x}_1 - \bar{x}_3$ and $\Delta\bar{y} = \bar{y}_1 - \bar{y}_2$, $\omega_0^2 = g/l$ and $\tau = \tau_i$.

In a single-pass interferometer the phase change is

$$\Delta\varphi = 4\pi(\Delta x - \Delta y)/\lambda\,,\tag{2.15}$$

where λ is the light wave length; hence, considering that, when the GW is propagating along the z axis, $h_{11}^{TT} = -h_{22}^{TT}$ and putting $\Delta\bar{\varphi} = 4\pi(\Delta\bar{x} - \Delta\bar{y})/\lambda$, we obtain

$$\Delta\ddot{\varphi} + \tau^{-1}(\Delta\dot{\varphi} - \Delta\dot{\bar{\varphi}}) + \omega_0^2(\Delta\varphi - \Delta\bar{\varphi}) = \frac{4\pi}{\lambda}\ddot{h}_{11}L\,.\tag{2.16}$$

This equation can be easily integrated giving [Pizzella 1975]

$$\Delta\varphi(t) = \frac{4\pi L}{\lambda\tilde{\omega}_0} \int\limits_0^t \sin\tilde{\omega}_0(t - \eta)\,e^{-(t-\eta)/2\tau}[\ddot{h}_{11}^{TT}(\eta) + \tau^{-1}\Delta\dot{\bar{\varphi}}(\eta) + \omega_0^2\Delta\bar{\varphi}(\eta)]\,d\eta\,,$$

$$\tilde{\omega}_0 = \sqrt{\omega_0^2 - 1/(4\tau^2)}\,.\tag{2.17}$$

To understand the effect of the GW on $\Delta\varphi$ we can neglect the seismic noise contribution and study the behaviour of eq. (2.17) assuming two simple functional forms for $h(t) = h_{11}^{TT}(t)$. In the first case we assume $h(t)$ to be a pulse of duration $\Delta t \ll 1/\omega_0$ and amplitude h_0,

$$h(\eta) = h_0[\theta(\eta) - \theta(\eta - \Delta t)] .\tag{2.18}$$

Inserting eq. (2.18) in eq. (2.17) and assuming the mechanical quality factor of the pendula $Q = \omega_0 \tau \gg 1$ we obtain

$$\Delta\varphi(t) = \frac{4\pi L}{\lambda} h(t) + \frac{4\pi L}{\lambda} h_0[\omega_0 \Delta t \sin(\omega_0 t) e^{-t/\tau} + O((\omega_0 \Delta t)^2) + O(1/Q^2)] .\tag{2.19}$$

Equation (2.19) shows that in the interferometric detector the measurement of $\Delta\varphi$ gives a precise measure of $h(t)$; the term in h_0, which represents the "memory" that the pendula have of the GW for $t > \Delta t$, can be neglected since it is multiplied by $\omega_0 \Delta t \ll 1$.

In the second case we consider a periodic GW with amplitude

$$h(t) = h_0 e^{-i\Omega_g t} .\tag{2.20}$$

Inserting $h(t)$ in eq. (2.17) we obtain for $t \gg \tau$

$$\Delta\varphi = -\frac{4\pi L}{\lambda} \frac{\Omega_g^2 e^{i\Omega_g t} h_0}{\omega_0^2 - \Omega_g^2 + i\Omega_g/\tau} .\tag{2.21}$$

For $\Omega_g > \omega_0$ and $Q \gg 1$, eq. (2.20) becomes

$$\Delta\varphi = (4\pi L/\lambda)/h_0 e^{i\Omega_g t} .\tag{2.22}$$

Equation (2.22) shows that with an interferometric detector it is possible to measure distortionless $h(t)$ even for a periodic GW; hence the very peculiarity of this detector is due to the low value of the pendulum resonance frequency ν_0, which can be made as low as a few Hz, giving the possibility, in principle, to detect low-frequency GWs. Furthermore the possibility of making L very large (some km), in virtue of eq. (2.9), would allow the operation of the antenna at room temperature while maintaining high sensitivity even in the presence of noise, such as thermal noise, which is dominant at low frequency.

For the evaluation of the phase shift due to the GW interaction of a photon beam bouncing between two mirrors, it is opportune to choose a coordinate system in which the mirrors are at rest; in this system the only GW interaction with the photon beam is due to the change of the metric coefficients. In fact if the mirrors are freely falling (i.e. with suspensions having no rigidity), then in the TT system they are at rest; this is easily shown considering that to first order in $h_{\alpha\beta}^{TT}$ from eqs. (2.2) and (2.4) it follows that

$$\Gamma^\alpha_{\beta\mu} \;\rightarrow\; \Gamma^\alpha_{\beta 0} = -\tfrac{1}{2}\dot{h}^{TT}_{\alpha\beta} , \qquad \frac{D^2\xi^\alpha}{d\tau^2} = \frac{d^2\xi^\alpha}{dt^2} - \tfrac{1}{2}\ddot{h}^{TT}_{\alpha\beta}\xi^\beta = -R^\alpha_{0\gamma0}\xi^\gamma = -\tfrac{1}{2}\ddot{h}^{TT}_{\alpha\beta}\xi^\beta , \tag{2.23}$$

and hence $(\ddot{\xi}^\alpha)_{TT} = 0$.

A matrix approach, used extensively for the evaluation of the phase shift due to the GW interaction with a photon bouncing between freely falling mirrors, is due to Vinet [1986]. The method is based on the consideration that due to eq. (2.23) the only effect of the GW on a photon is contained in the perturbed ds^2,

$$ds^2 = c^2 \, dt^2 - [1 + h(t)] \, dx^2 - [1 - h(t)] \, dy^2 , \tag{2.24}$$

where $h(t) = h \cos \phi$, with $\phi = \Omega_g t + \varphi$ and the photon is supposed to travel along the x or y axis.

If the photon is scattered back by a mirror at distance $x = L$, then from eq. (2.24) it follows that the round trip retarded time is

$$t_r = t - \frac{2L}{c} - \varepsilon h \, \frac{L}{c} \, \frac{\sin \eta}{\eta} \cos(\phi - \eta) , \tag{2.25}$$

where $\eta = \Omega_g L / c$ and $\varepsilon = \pm 1$ if the photon is traveling along x or y, respectively.

If the time dependent part of the EM fields along the trajectory is taken to be

$$A(t) = (A_0 + \tfrac{1}{2} h \, e^{i\phi} A_1 + \tfrac{1}{2} h \, e^{-i\phi} A_2) \, e^{-i\omega t} , \tag{2.26}$$

where $\omega = 2\pi\nu_0$ (ν_0 is the laser frequency) then substitution of eq. (2.25) in eq. (2.26) gives (to first order in h)

$$A(t) = e^{i\omega(2L/c - t)} \left[A_0 + \tfrac{1}{2} h \, e^{i\phi} \left(A_1 \, e^{-2i\Omega_g L/c} + i\omega\varepsilon \, \frac{L}{c} \, \frac{\sin \eta}{\eta} \, e^{-i\eta} A_0 \right) \right.$$

$$\left. + \tfrac{1}{2} h \, e^{-i\phi} \left(A_2 \, e^{2i\Omega_g L/c} + i\omega\varepsilon \, \frac{L}{c} \, \frac{\sin \eta}{\eta} \, e^{i\eta} A_0 \right) \right] . \tag{2.27}$$

This can be put in matrix form,

$$\begin{pmatrix} A_0 \\ A_1 \\ A_2 \end{pmatrix}' = D \begin{pmatrix} A_0 \\ A_1 \\ A_2 \end{pmatrix} , \tag{2.28}$$

$$D = x \begin{pmatrix} 1 & 0 & 0 \\ i\varepsilon\xi \, \dfrac{\sin \eta}{\eta} \, e^{-i\eta} & \bar{y} & 0 \\ i\varepsilon\xi \, \dfrac{\sin \eta}{\eta} \, e^{i\eta} & 0 & y \end{pmatrix} , \tag{2.29}$$

$\xi = \omega L / c$, $x = e^{2i\xi}$, $y = e^{2i\eta}$.

This approach can be applied to interferometric GW detectors because in this kind of antenna the observation frequency is always above the mirror suspension mode frequencies, hence the mirrors can be considered as being freely falling.

The case of mirrors elastically bound with self-frequency $\nu_m = \Omega_m / 2\pi$ has been treated by Pegoraro

et al. [1978]; they found a gauge transformation

$$\varepsilon^0 = \frac{1}{2c} \lambda \dot{h}_{\alpha\beta}^{TT} x^\alpha x^\beta , \qquad \varepsilon^3 = \frac{1}{2c} \lambda \dot{h}_{\alpha\beta}^{TT} x^\alpha x^\beta ,$$

$$\varepsilon^\alpha = -\lambda h_{\alpha\beta}^{TT} x^\beta , \qquad \beta, \alpha = 1, 2 ,$$ (2.30)

$$\lambda = \tfrac{1}{2}\Omega_m^2/(\Omega_m^2 - \Omega^2) , \qquad \Omega \neq \Omega_m ,$$ (2.31)

giving a $h_{\mu\nu}$, evaluated by means of eq. (1.9), which leaves at rest a mirror initially at rest.

An eikonal equation expansion to first order in $h_{\mu\nu}$ has been studied by Linet and Tourrenc [1976]; they found that the photon phase shift can be put in the form

$$\varphi = \frac{c^2}{\hbar E} \int_{t_0}^{t_1} h_{\mu\nu} p^\mu p^\nu \, dt ,$$ (2.32)

where p^μ is the photon four-momentum, and showed that in the resonance arising from the GW and photon interaction [Braginskii and Menskii 1971, Braginskii et al. 1974] the photon phase shift increases linearly with time and is proportional to the ratio ω/Ω_g.

3. Delay line interferometers

The need to increase the interferometer phase shift due to a GW signal is dictated by the existence of noise which affects only the phase of the optical rays without creating real displacements of the mirrors. To overcome the effects due to this noise, which will be called "phase noise" in contrast to "displacement noise", it is very important to find an optical scheme allowing the beams to bounce back and forth in the optical cavities.

Actually the ultimate phase noise is the photon counting noise $\Delta\phi_{PC}(t)$ due to the anticorrelated fluctuations Δn of the photon number n in the interferometer arms according to the uncertainty relation

$$\langle \Delta\phi_{PC}(t)^2 \rangle^{1/2} = \Delta\phi_{PC} \geq 1/\Delta n .$$ (3.1)

For a photon coherent state $\Delta n = \sqrt{n}$, hence

$$\Delta\phi_{PC} \geq 1/\sqrt{n} = \sqrt{h\nu_0/W_{eff}t} ,$$ (3.2)

where h is Planck's constant, ν_0 the laser frequency, W_{eff} the light power in the interferometer arms and t the measurement time. If the light makes $2N$ reflections (see fig. 3.1), the phase shift due to a mirror displacement $\Delta x_{1,2} = \pm\tfrac{1}{2}h(t)L$ is

$$\varphi_{1,2} = \frac{4N\pi}{\lambda} \Delta x + \bar{\varphi}_{1,2} = \varphi_s/2 + \bar{\varphi}_{1,2} ,$$ (3.3)

where $\bar{\varphi}_{1,2}$ are given fixed phase shifts in the two arms and Δx has been evaluated in the limit $\Omega_g L/c \ll 1$.
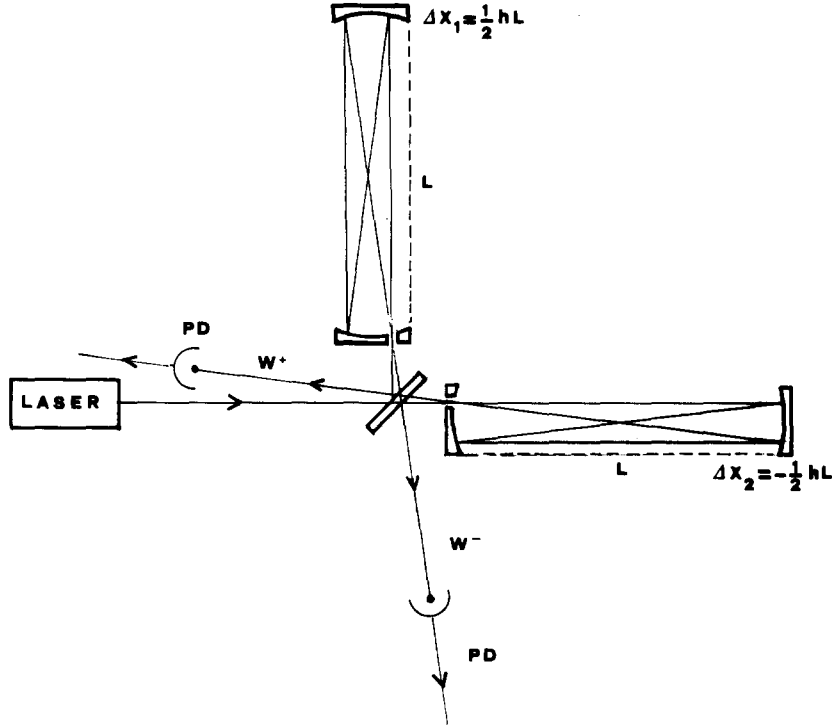
Fig. 3.1. In the delay line scheme, the laser beam enters the two optical cavities and bounces $2N$ times between the mirrors with the purpose to increase the S/N ratio of the GW signal to the photon counting noise.

With reference to fig. 3.1 the power of the recombined beams is

$$W_\pm = R^{4N}(W/2)[1 \pm \cos(\varphi_s + \varphi_0 + \Delta\phi_{PC})] ,$$ (3.4)

where R^2 is the intensity reflectivity of the mirrors, $\varphi_0 = \bar{\varphi}_1 - \bar{\varphi}_2$ and $\Delta\phi_{PC}$ has been evaluated for $W_{eff} = WR^{4N}$. Putting $\varphi_0 = \pi/2$, measuring $W_\pm$ with photodiodes PD having efficiency η and forming the current difference, we obtain

$$\Delta I^2 \cong I_0^2\{[(4N\pi/\lambda)h(t)L]^2 + \Delta\phi_{PC}^2\} + \Delta I_{SN}^2 ,$$ (3.5)

where

$$I_0 = (We/h\nu_0)\eta R^{4N} \quad \text{and} \quad \Delta I_{SN} = e\sqrt{(WR^{4N}/th\nu_0)\eta(1 - \eta)}$$

are the photodiode mean current and current fluctuation, respectively; e is the electric charge. The GW detection condition, introducing eq. (3.2) in eq. (3.5) and using eq. (3.3), reads

$$h(t) > \frac{\lambda}{4N\pi L} \sqrt{\frac{h\nu_0}{Wt\eta R^{4N}}} ,$$ (3.6)

where the assumption $2\Omega_g NL/c \ll 1$ has been made. Equation (3.6) shows that $2N$ reflections increase accordingly the S/N ratio for the photon counting noise.

The delay line (DL) scheme was first studied by Herriot et al. [1964]; the laser beam enters the cavity through a hole in the near mirror with coordinate (x_0, y_0) and slope (x'_0, y'_0) (see fig. 3.2) and is reflected back and forth between the mirrors having distance L and focal length f, respectively. Defining

$$\cos \theta = 1 - L/2f \, , \tag{3.7}$$

where θ is the rotation angle of the beam spot on the mirrors (see fig. 3.3), the coordinates of the nth spot are

$$x_n = x_0 \cos n\theta + \sqrt{\frac{L}{4f - L}} \, (x_0 + 2fx'_0) \sin n\theta \, ,$$

$$\tag{3.8}$$

$$y_n = y_0 \cos n\theta + \sqrt{\frac{L}{4f - L}} \, (y_0 + 2fy'_0) \sin n\theta \, , \quad 4f - L > 0 \, ,$$
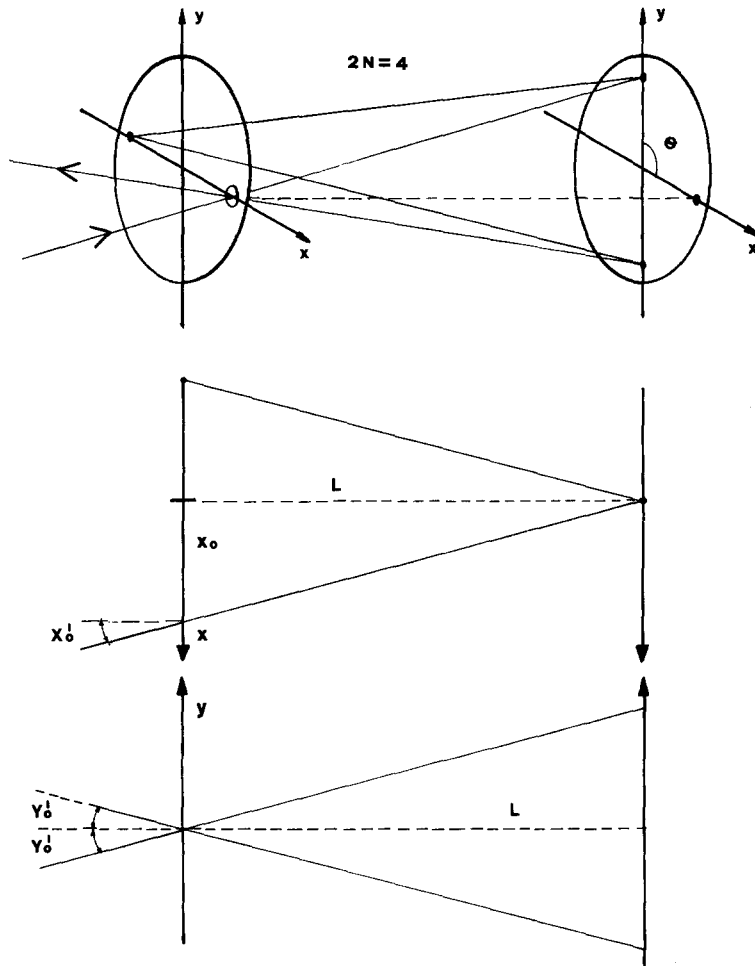
Fig. 3.2. The laser beam enters the DL at position (x_0, y_0) and angle (x'_0, y'_0), then bounces $2N$ times and leaves the cavity through the entrance hole.

● Spot on the close mirror
○ Spot on the far mirror
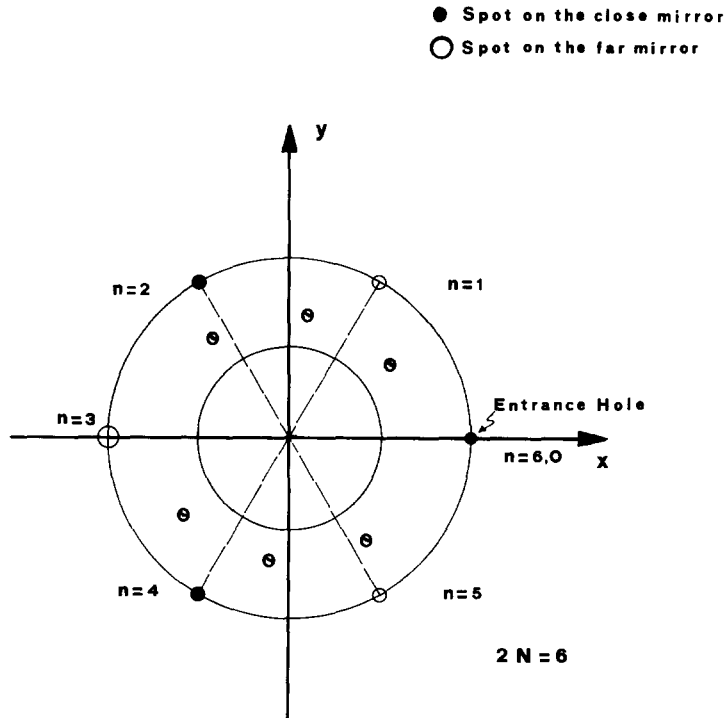
Fig. 3.3. The beam enters the DL at position $n = 0$, is reflected from the far mirror at positions $n = 1, 3, 5$ and from the close one at positions $n = 2, 4$. $2N\theta$ can be larger than 2π.

which can be put in the form

$$x_n = A \sin(n\theta + \alpha) , \qquad y_n = B \sin(n\theta + \beta) , \tag{3.9}$$

where

$$A^2 = \frac{4f}{4f - L} [x_0^2 + L x_0(x_0') + L f(x_0')]^2 , \qquad \mathrm{tg}\, \alpha = \sqrt{\frac{4f}{L} - 1} \; \frac{1}{1 + 2f x_0'/x_0} , \tag{3.10}$$

and similarly for B and β. If $A = B$ the spots lie on a circle; the beam reentrance condition is fulfilled when

$$2k\theta = 2J\pi , \quad J, k \text{ integers}, \ J \neq k , \tag{3.11}$$

k being the number of spots on a single mirror.

The DL is a very flexible method to cope with misalignments due to mirror movements [Goorvitch 1975, Billing et al. 1979]. Fattaccioli et al. [1986] have shown that the total optical phase shift is independent of tilting ($\Delta\vartheta$) and transverse mutual mirror translations (Δx) up to second order in $\Delta x/R$ and $\Delta\vartheta$, respectively, R being the radius of the spot circle on the mirrors, if the DL is perfectly reentrant and aligned.

With the purpose of reducing the light scattering from the entrance hole in the mirrors close to the

beam splitter [Schilling et al. 1981], the size of the input beam should be sufficiently reduced increasing the beam angular spread $\Delta x'_c$ and $\Delta y'_c$. The spot diameters due to this spread,

$$\Delta x_n = \sqrt{\frac{L}{4f-L}}\, 2f \sin n\theta\, \Delta x'_0 , \qquad \Delta y_n = \sqrt{\frac{L}{4f-L}}\, 2f \sin n\theta\, \Delta y'_0 , \qquad (3.12)$$

do not increase indefinitely with N but vary cyclically with n; this focusing characteristic is very relevant for avoiding beam size divergence when N is large, and a careful evaluation of the beam entrance parameters is needed to avoid geometrical overlapping of the spots. Actually two contiguous spots on a mirror are associated with different delays; if they do overlap the light diffused by the mirror coatings is sent in the wrong beam, causing noise due to the finite size of the laser line width.

The light phase shift due to GW interaction in a DL without the constraint $2\Omega_g NL/c \ll 1$ has been calculated by Vinet [1986] and Vinet et al. [1988].

Let us consider a DL of length L in which the beam is reflected $2N$ times and which has mirrors with amplitude reflectivity iR_1 and iR_2. By repeated application of the operator D [see eq. (2.29)] we obtain the $2N$ reflection operator,

$$iM = (iR_1)^{N-1}(iR_2)^N D^N = (-)^{N-1} R_1^{N-1} R_2^N x^N \begin{pmatrix} 1 & 0 & 0 \\ i\varepsilon\xi\, \dfrac{\sin\eta N}{\eta}\, e^{-i\eta} & y^{-N} & 0 \\ i\varepsilon\xi\, \dfrac{\sin\eta N}{\eta}\, e^{i\eta} & 0 & y^N \end{pmatrix}, \qquad (3.13)$$

where the signal is contained in the two matrix elements M_{12} and M_{13}; putting

$$\tau_s = 2NL/c , \qquad (3.14)$$

we see that M_{12} and M_{13} are maximum when

$$\eta N = \tfrac{1}{2}\Omega_g \tau_s = \pi/2 , \qquad (3.15a)$$

while the signal is zero when

$$\tfrac{1}{2}\tau_s\Omega_g = n\pi \quad (n = 1, 2, \ldots) . \qquad (3.15b)$$

From eqs. (2.27) and (3.7) it follows that the maximum phase shift $\Delta\phi_{DL}$ of the light wave due to GW interaction in two DLs (see fig. 3.1) is

$$\Delta\phi_{DL} = 2h\omega\, \frac{L}{c}\, \frac{\sin \Omega_g(L/c)N}{\Omega_g L/c} . \qquad (3.16)$$

Typical DL schemes are those adopted by Forward [1978] at Malibu with $2N = 4$, MIT with $2N = 56$ and Max-Planck-Institut in Munich with $2N \cong 90$.
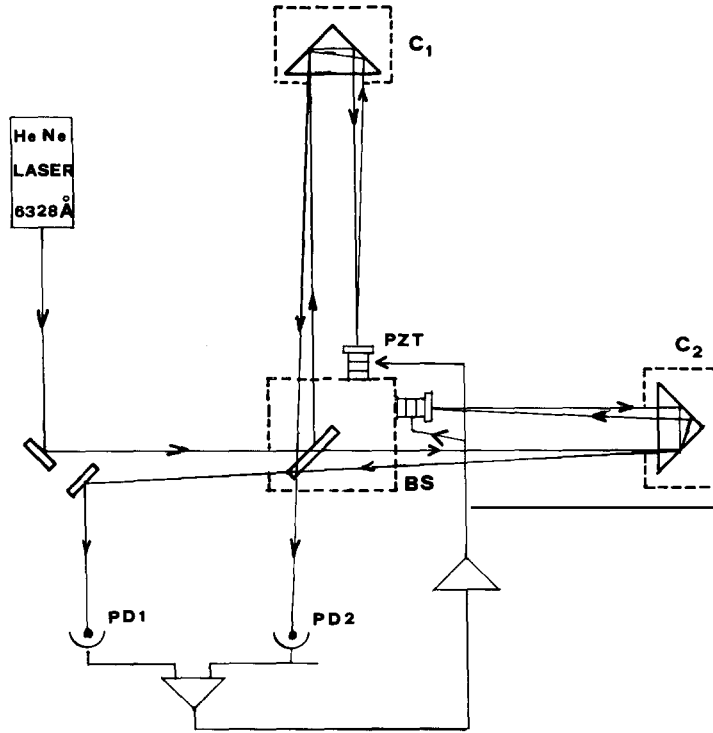
Fig. 3.4. The optical layout of the Malibu interferometer. The beam splitter BS is mounted on the central mass where the piezoelectric transducers PZT, driven by the filtered difference signal of the photodetectors PD1 and PD2, keep the interferometer output locked to null. The retroreflectors C1 and C2 are mounted on the far masses, which are ~2 m away from BS. The detector is lit by a 30–50 mW HeNe laser.

In the Malibu interferometer, the world's first working prototype, the optical system (see fig. 3.4) is composed of a beam splitter and two retroreflectors mounted on the far masses. The optical path is ~8 m and the strain sensitivity is $\tilde{h} \gtrsim 10^{-16}\,\mathrm{Hz}^{-1/2}$ for $\nu \gtrsim 2\,\mathrm{kHz}$.

The MIT interferometer, shown in fig. 3.5, is a system with $2N = 56$ and a mirror separation of 1.46 m. The mass supporting the beam splitter also supports two Pockels cells used both for keeping the interferometer locked to a fringe and for giving phase modulation with the purpose of reducing the laser amplitude noise. The noise due to the laser lateral beam jitter is reduced by transporting the laser light through an optical fiber. The mirror's pendulum oscillations are damped by means of electrostatic dampers [Linsay and Shoemaker 1982]. The strain sensitivity obtained [Livas et al. 1986] is $\tilde{h} \simeq 3 \times 10^{-17}\,\mathrm{Hz}^{-1/2}$.

In the Munich interferometer (see fig. 3.6) the mirror distance can be adjusted between 29 m and 32 m with the purpose of obtaining different numbers of beams. Locking to a fringe is obtained both by using Pockels cells inserted in the DL and a magnet and coil [Billing et al. 1979] damping system on the mirrors; more details about the use of these systems will be given in subsequent sections. The laser is a 5 W argon ion laser stabilized by means of an external reference cavity and by the interferometer itself used as a reference cavity. The laser light is fed to the interferometer by means of an optical fiber. The maximum sensitivity achieved [Shoemaker et al. 1987a] with $2N = 90$ is $\tilde{h} \simeq 8 \times 10^{-20}\,\mathrm{Hz}^{-1/2}$.
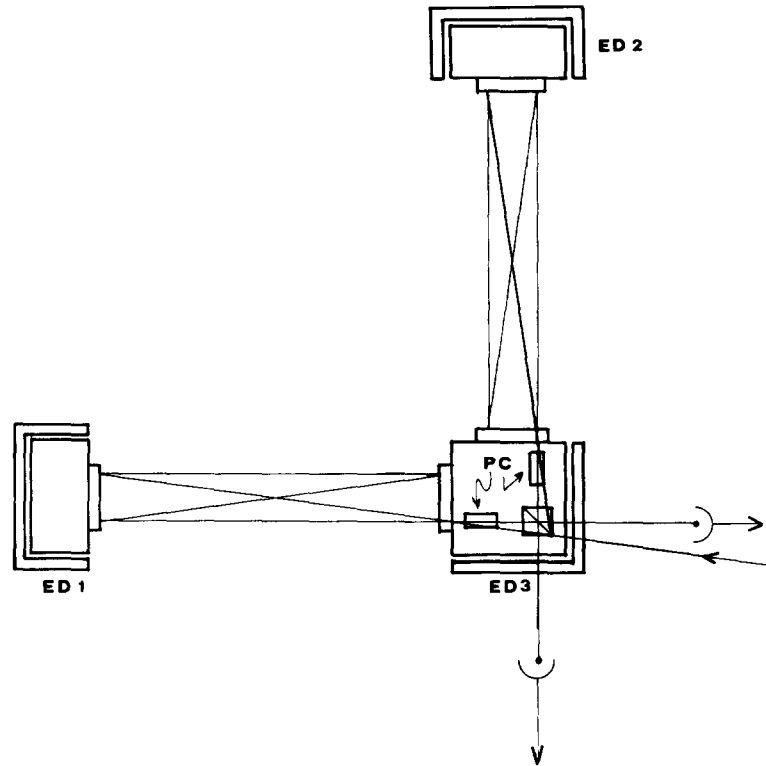
Fig. 3.5. The MIT interferometer: a DL system with $2N = 56$ and 1.46 m long arms. The optical phase is locked by means of Pockels cells PC mounted on the beam splitter. An optical fiber is used to feed the laser light and to reduce the laser lateral beam jitter. The pendulum motions of the masses are damped by means of the electrostatic dampers ED.
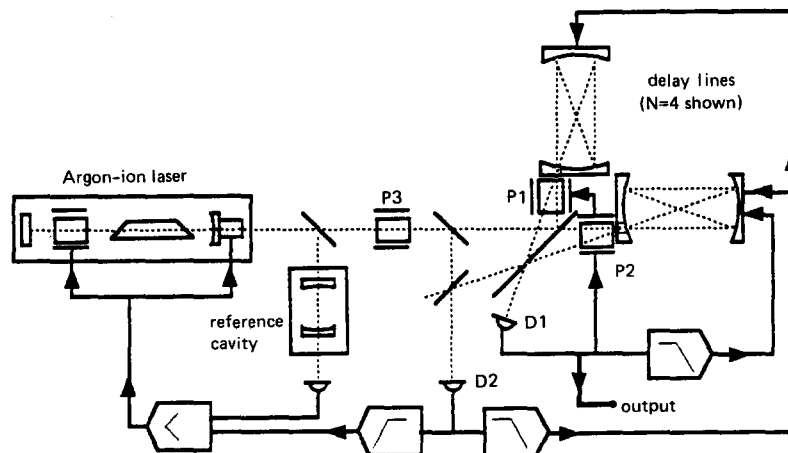
Fig. 3.6. Layout of the Munich interferometer (from Shoemaker et al. [1987a]) showing the laser stabilization scheme. The laser is locked both to the reference cavity and the interferometer itself used as a frequency reference. Locking of the interferometer to a fringe and phase modulation are performed by the Pockels cells P1 and P2. Magnets and coils are used to damp the pendulum oscillations of the mirrors.

4. Fabry–Pérot interferometers

Fabry–Pérot (FP) theory is largely described in many books (see, for example, Born and Wolf [1964], Hernandez [1986]); with reference to fig. 4.1, M_1 and M_2 are two mirrors located at positions x_1 and x_2, respectively ($x_2 - x_1 = L$); the amplitude reflectance iR_i, the transmittance T_i and the loss B_i of the mirrors satisfy the relation

$$T_i^2 + R_i^2 + B_i^2 = 1, \quad i = 1, 2.$$ (4.1)

A light beam of frequency $\nu_0 = \omega_0 / 2\pi$ entering the cavity with amplitude A_0 is partially transmitted with amplitude A_t and partially reflected with amplitude A_r.

If A_2 and A_3 are the transmitted and reflected amplitudes inside the cavity, then

$$A_r = iR_1 A_0 + T_1 A_3, \qquad A_2 = T_1 A_0 + iR_1 A_3, \qquad A_3 = iR_2 D A_2,$$ (4.2)

where D is defined in eq. (2.29). The solution is

$$A_r = i[R_1 + (R_1^2 + T_1^2)R_2 D](1 + R_1 R_2 D)^{-1} A_0 = iF A_0.$$ (4.3)

An evaluation of F gives the relevant matrix elements [Vinet 1986],

$$F_{11} = i \frac{R_1 + (R_1^2 + T_1^2)R_2 x}{1 - R_1 R_2 x},$$

$$F_{21} = \frac{\varepsilon T_1^2 R_2 \xi \sin(\eta)/\eta}{1 - R_1 R_2 x} \frac{e^{-i\eta}x}{1 - R_1 R_2 x\bar{y}},$$ (4.4)

$$F_{31} = \frac{\varepsilon T_1^2 R_2 \xi \sin(\eta)/\eta}{1 - R_1 R_2 x} \frac{e^{i\eta}x}{1 - R_1 R_2 xy},$$

where x and y have been defined in eq. (2.29).

From eqs. (2.27) and (4.4) it is possible to evaluate the maximum phase shift $\Delta\phi_{FP}$ for a cavity configuration similar to the one shown in fig. 3.1 under the condition $x = +1$ (optical resonance condition),

$$\Delta\phi_{FP} = 2 \frac{T_1^2 R_2 h\omega L/c}{(1 - R_1 R_2)^2} \frac{1}{\sqrt{1 + F' \sin^2 \Omega_g L/c}},$$ (4.5)
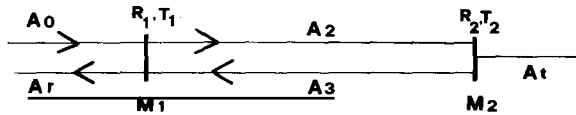
Fig. 4.1. Schematic diagram of the light field amplitudes inside a cavity, composed of the mirrors M_1 and M_2 having reflectivity iR_1 and iR_2 and transmittance T_1 and T_2, respectively. The amplitude A_3 is connected to A_2 through the operator defined in eq. (2.29) containing the effect due to the GW interaction.

where $F' = 4R_1R_2/(1 - R_1R_2)^2$, $T_2 \ll T_1$ and the realistic condition $\Omega_g L/c \ll 1$ has been assumed. In analogy to eq. (3.8), defining the cavity storage time

$$\tau_s = 2 \frac{L}{c} \frac{\sqrt{R_1R_2}}{1 - R_1R_2},$$ (4.6)

making the approximation $R_i \cong 1 - \frac{1}{2}(T_i^2 + B_i^2)$ and putting $B_i \ll T_i$ we finally obtain

$$|\Delta\phi_{FP}| \cong \omega h\tau_s \frac{2T_1^2}{T_1^2 + T_2^2} \sqrt{\frac{R_2}{R_1}} \frac{1}{\sqrt{1 + \Omega_g^2\tau_s^2}}.$$ (4.7)

The comparison between $|\Delta\phi_{DL}|$ and $|\Delta\phi_{FP}|$ is shown in fig. 4.2; $|\Delta\phi_{FP}|$ is plotted for $T_2 \ll T_1$; this experimental condition is particularly useful in interferometers using light recycling because very little power flows out of the far mirror.

Effects due to misalignment of the FP cavity have been evaluated by Fattaccioli et al. [1986].

Typical FP prototype interferometers are in Glasgow and at CALTECH. The Glasgow interferometer [Ward et al. 1987] (see fig. 4.3) is composed of two 10 m long cavities. The laser is frequency locked to one of the cavities; this is achieved by adjusting the laser frequency by means of a piezoelectrically driven mirror and an intracavity Pockels cell. The length of the second cavity is then adjusted by means of forces produced by magnets connected to the mirrors pushed by electrical coils, and maintained in resonance with the first one by means of a servo loop. The GW signal is obtained from the electronically recombined arm beams. With 30 mW light power the strain sensitivity [Ward et al. 1987] was 1.2×10^{-19} Hz$^{-1/2}$ for frequencies greater than 1500 Hz.

The CALTECH interferometer [Spero 1986] has two 40 m long cavities; one of them is used to frequency stabilize the laser by means of an intracavity Pockels cell and the other cavity is kept in
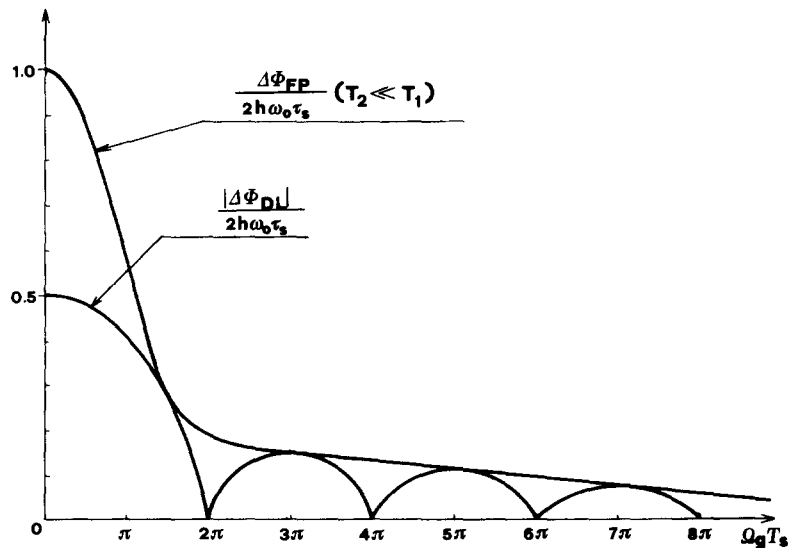
Fig. 4.2. Comparison between the phase shift due to the GW amplitude h of a FP ($T_2 \ll T_1$) and a DL interferometer having the same storage time τ_s. When $\Omega_g \tau_s \gg 1$ the phase shifts are comparable, as is shown by eqs. (4.7) and (3.16).
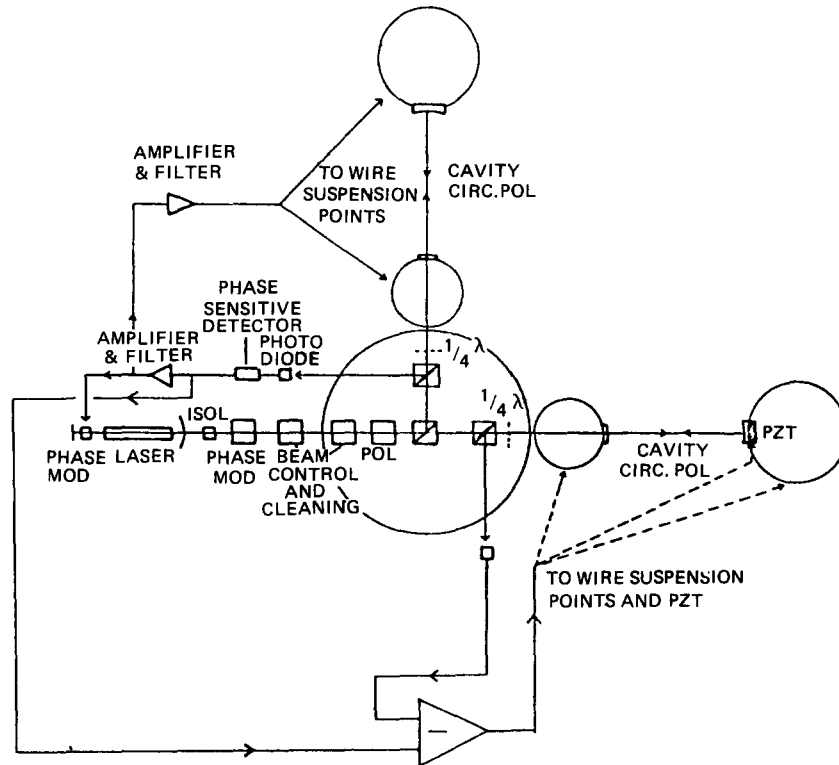
Fig. 4.3. The Glasgow interferometer (from Newton et al. [1986]). One of the two 10 m FP cavities is used for stabilizing the laser; the other is, via a feedback system, kept in resonance with the laser frequency. The GW signal is contained in the feedback signal.

resonance with the first one by means of forces applied to the mirrors. The strain sensitivity with a light power of 2 mW was $\tilde{h} \cong 5 \times 10^{-19}\,\mathrm{Hz}^{-1/2}$ [Spero 1986].

Optical recombination of the two beams has been achieved in Orsay by Man et al. [1986] with a phase sensitivity of $1.5 \times 10^{-8}\,\mathrm{rad}\,\mathrm{Hz}^{-1/2}$.

5. The noise due to photon counting errors and recycling

In section 3 we have shown how the phase fluctuations in the two interferometer arms produce noise; in particular the fluctuations of the photodiode currents [see eq. (3.5)] ΔI_{SN} have been considered as a source of photon counting errors. But also if $\Delta I_{\mathrm{SN}} = 0$ ($\eta = 1$) the interferometer's output current still fluctuates. To explain this fact it was necessary to make an accurate analysis of the photon beam–beam splitter interaction.

Two approaches lead to the same result: in the first [Edelstein et al. 1978] the beam splitter is shown to create two anticorrelated photon beams having n_1 and n_2 photons each, in such a way that the difference of the photon number fluctuations Δn_1 and Δn_2 in the two beams does not cancel even when $\bar{n}_1 = \bar{n}_2$. In the second approach [Caves 1980] the zero point vacuum fluctuations of the photon field entering from the open beam splitter port (see fig. 5.1) produce anticorrelated photon number fluctuations in the interferometer arms.

The rms fluctuations $\Delta n_i^2 = n_i$ produce both phase noise $\Delta\phi_{\mathrm{PC}} \simeq 1/\sqrt{n}$, where $n = n_1 + n_2$, and a
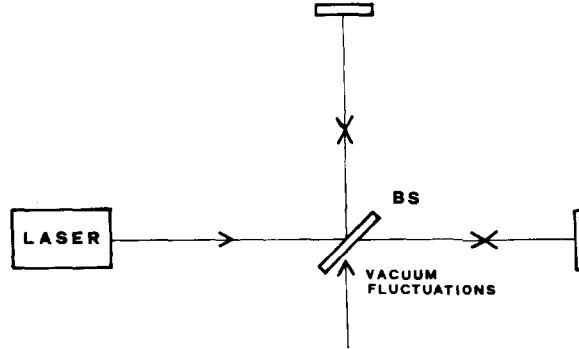
Fig. 5.1. The light field vacuum fluctuations entering the unused port of the beam splitter BS produce the anticorrelated intensity fluctuations in the interferometer arms.

fluctuation in the differential radiation pressure on the interferometer's mirrors, which produces the differential momentum $\Delta P = \sqrt{n}\,(h\nu_0/c)\,2N$.

The equivalent displacement noise producing the phase shift $\Delta\phi_{PC}$ is $\Delta x_{PC} = (\Delta\phi_{PC}/2N)\lambda/4\pi$; hence in the measurement time t the total displacement $\sqrt{\Delta x_{PC}^2 + (\Delta P\,t/2M)^2}$ is minimum when

$$W = (4N^2)^{-1} Mc^2/\omega t^2 \, . \tag{5.1}$$

The existence of this optimal laser power relies on the fact that the photon number fluctuations are anticorrelated in the two interferometer arms. The minimum displacement is

$$\Delta x_{QL} = \sqrt{h\,4\pi t/M} \, , \tag{5.2}$$

which is very close to the standard quantum limit for the accuracy with which the displacement of a mass M can be measured in a time t.

As we have seen in section 3, in a multireflection interferometer the h sensitivity, with respect to the photon counting error, increases with the number of reflections, with the arm length and with the effective detected power. Using eqs. (3.2) and (3.16) we see that the best sensitivity in h for a DL system is obtained when $\tau_s = \frac{1}{2}T_g$,

$$h_{DL} > \frac{1}{2\nu_0 T_g}\sqrt{\frac{h\nu_0}{\eta W T_g R^{4N}}} \, , \tag{5.3}$$

where T_g is the GW pulse length.

If the GW is periodic the sensitivity increases with the square root of the number of cycles observed. If $\frac{1}{2}\Omega_g\tau_s \ll 1$, eq. (5.3) becomes

$$h_{DL} > \frac{1}{\omega\tau_s}\sqrt{\frac{h\nu_0}{\eta W t R^{4N}}} \, . \tag{5.4}$$

Analogously for a FP system, from eqs. (3.2) and (4.7) we obtain

$$h_{FP} > \frac{1}{\omega} \frac{T_1^2 + T_2^2}{2T_1^2} \sqrt{\frac{R_1}{R_2}} \frac{\sqrt{1 + \Omega_g^2 \tau_s^2}}{\tau_s} \sqrt{\frac{h\nu_0}{\eta Wt}} \; .$$

For $T_2 \ll T_1$, $(R_1/R_2)^{1/2} \cong 1$, and $\Omega_g \tau_s > 1$, eq. (5.5) becomes

$$h_{FP} > \frac{1}{2\nu_0 T_g} \sqrt{\frac{h\nu_0}{\eta WT_g}} \cong h_{DL} \; . \tag{5.6}$$

The difference between eqs. (5.3) and (5.6) lies in the fact that for the FP case, unlike the DL case, the maximum sensitivity is obtained for any $\tau_s > 1/\Omega_g$. If $\Omega_g \tau_s < 1$, eq. (5.5) becomes

$$h_{FP} > \frac{1}{2\omega\tau_s} \sqrt{\frac{h\nu_0}{\eta WT}} \cong \tfrac{1}{2} h_{DL} \; . \tag{5.7}$$

It has also been shown [Edelstein et al. 1978] that maximum sensitivity occurs when the signal is taken from one of the photodiodes with the illuminating beam brought to extinction. The argument runs as follows. Equation (3.4) gives the current

$$I_- = \tfrac{1}{2} I_0 [1 - \cos(\varphi_0 + \varphi_s)] \; , \tag{5.8}$$

the current ΔI_s due to the signal being

$$\Delta I_s \cong \tfrac{1}{2} I_0 (\sin \varphi_0) \varphi_s \; .$$

The current fluctuations are the sum of the Poissonian beam fluctuations and the statistical fluctuations due to the diode detection inefficiency $1 - \eta$ [see eq. (3.5)], i.e.,

$$\Delta I^2 = e[\eta I_0 (1 - \cos \varphi_0)/2t + (1 - \eta) I_0 (1 - \cos \varphi_0)/2t] = e \frac{I_0 (1 - \cos \varphi_0)}{2t} \; , \tag{5.9}$$

where t is the measurement time. The measurability condition for φ_s reads $\Delta I_s^2 \geq \Delta I^2$, hence

$$h > \frac{\lambda}{4N\pi L} \sqrt{\frac{h\nu_0}{\cos^2(\tfrac{1}{2}\varphi_0) WR^{4N}\eta t}} \; , \tag{5.10}$$

which is minimum for $\varphi_0 = 0$ [see eq. (3.6)], i.e. when the beam is extinguished.

From this condition, using eq. (3.4), putting $\bar{\varphi}_1 - \bar{\varphi}_2 = \varphi_0 \ll 1$ and with $\varphi_s = (4N\pi/\lambda)h(t)L \ll 1$, it follows that the two light beams have the intensities

$$W_\pm \cong \tfrac{1}{2} R^{4N} W[1 \pm (\cos \varphi_0 - \varphi_s \sin \varphi_0)] \; , \tag{5.11}$$

where we have chosen the relative fixed phase in such a way as to have $W_+ = R^{4N}W$ going toward the laser. This light can be recycled [Drever 1982] according to the scheme of fig. 5.2. In this arrangement the beam W_+ is recycled by means of the mirrors BSR and MR. The position of the latter, and hence the phase shift, is changed by the transducer PZT driven by the PD2 signal.
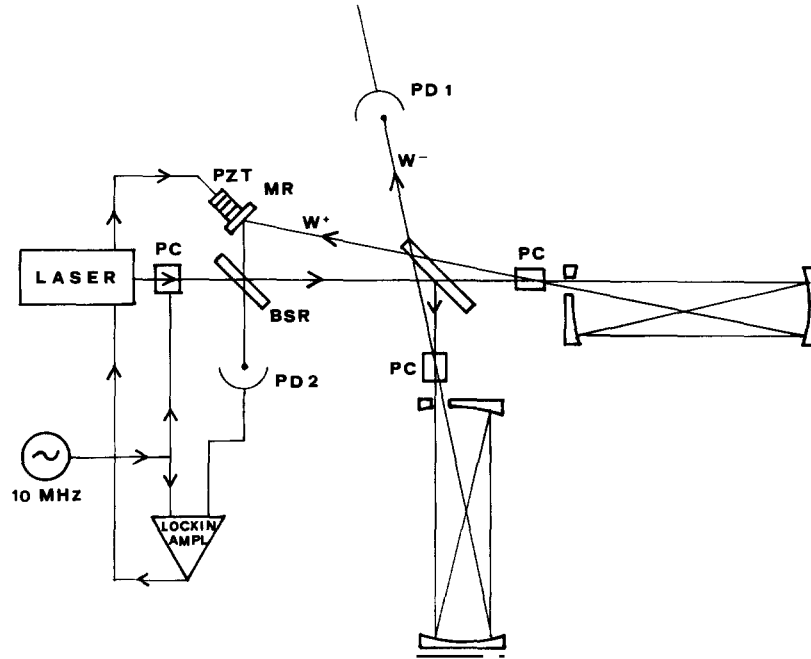
Fig. 5.2. The beam W_- can be brought to extinction by means of the Pockels cells PC; then W_+ is maximum and can be reused when MR gives the right phase shift. This is obtained by displacing MR by means of the piezoelectric transducer PZT driven by the signal of PD2.

To evaluate the power increase due to recycling in a DL, let us consider that the typical energy loss per cycle is

$$\Delta W = (1 - R^{4N})W \ . \tag{5.12}$$

The maximum sensitivity in a DL system occurs for $\tau_s = 1/(2\nu_g)$ and since

$$R^{4N} \cong 1 - 2(\pi c/L\Omega_g)(1 - R^2)/2 \ , \tag{5.13}$$

it follows that

$$W_R = WL\Omega_g/\pi c(1 - R^2) \ . \tag{5.14}$$

Hence, from eq. (5.13) it follows that the overall power gain is a function of Ω_g and the sensitivity in h [see eq. (5.3)] becomes

$$(h_{DL})_R = \sqrt{\frac{(1 - R^2)\pi c}{L\Omega_g}} \ h_{DL} = \frac{1}{2} \sqrt{\frac{h\lambda\pi(1 - R^2)\nu_g}{R^{4N}\eta WL4\pi T_g}} \ . \tag{5.15}$$

Let us now evaluate the analog of eq. (5.14) in case of a FP system. The schematic diagram of fig. 5.3 shows that in the FP recycling scheme the recycling mirror MR is positioned directly in the laser beam. The correct phase, obtained by driving the PZT with the signal of the photodiode PD2, gives a minimum signal in PD2. In analogy with the DL system we evaluate the light power lost in the mirror
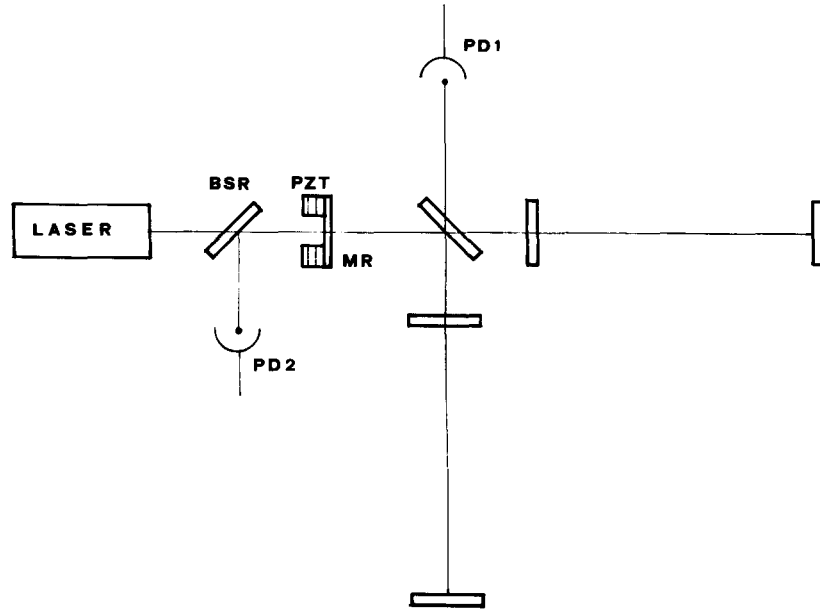
Fig. 5.3. The power recycling scheme for a FP interferometer. In analogy to the scheme of fig. 5.2 the signal of the photodiode PD2 is used to displace the mirror MR in such a way as to have minimum illumination of PD2.

collision; let us suppose that $T_2 \ll T_1$; in this case the reflected amplitude is, at optical resonance,

$$A_r \cong \frac{-R_1 + R_1^2 + T_1^2}{1 - R_1} A_0 i .$$

(5.16)

Using the equation $R_1^2 + T_1^2 + B_1^2 = 1$, it follows that

$$A_r = A_0[1 - B_1^2/(1 - R_1)]i .$$

(5.17)

In a single mirror hit the power loss is

$$\Delta W \cong -W \cdot 2B_1^2/(1 - R_1) .$$

(5.18)

Hence, if we attribute the whole loss to the near mirror, the power enhancement due to recycling should be

$$W_R \cong W(1 - R_1)/2B_1^2 .$$

(5.19)

Since the storage time in the cavities should be comparable to the recycling time and because it is convenient to have $\Omega_g \tau_s = 1$, it follows that

$$\tau_s = \frac{2L}{c} \frac{\sqrt{R_2 R_1}}{1 - R_1 R_2} = \frac{1}{\Omega_g} .$$

(5.20)

Since, for the sake of simplicity, we have put $R_2 = 1$, then

$$1 - R_1 \cong 2L\Omega_g/c . \tag{5.21}$$

This gives

$$W_R = WL\Omega_g/cB_1^2 , \qquad (h_{FP})_R \cong h_{FP}(B_1^2 c/L\Omega_g)^{1/2} . \tag{5.22}$$

Experimental results on power recycling have been obtained by Rüdiger et al. [1987] using a simple 0.3 m arm DL interferometer having $2N = 2$. A recycling factor of up to 15 was obtained with a total power of 2 W.

Similar results were obtained in Orsay (Man et al. [1987]). It was shown that the recycling factor was limited by the loss in the Pockels cells situated in the arms of the interferometer. Better results were obtained later using the external modulation technique (see below).

It has been pointed out [Ruggiero 1979, Drever 1981] that it is possible to increase the signal phase shift by allowing the photons to go synchronously with a periodical GW from one cavity to the other, when the cavities have $\tau_s = \pi(2n + 1)/\Omega_g$ (n integer). This method is called synchronous recycling (SR). The laser beam (see fig. 5.4) is split by the mirror M_0 and the light enters the two DLs from M_1; in M_2
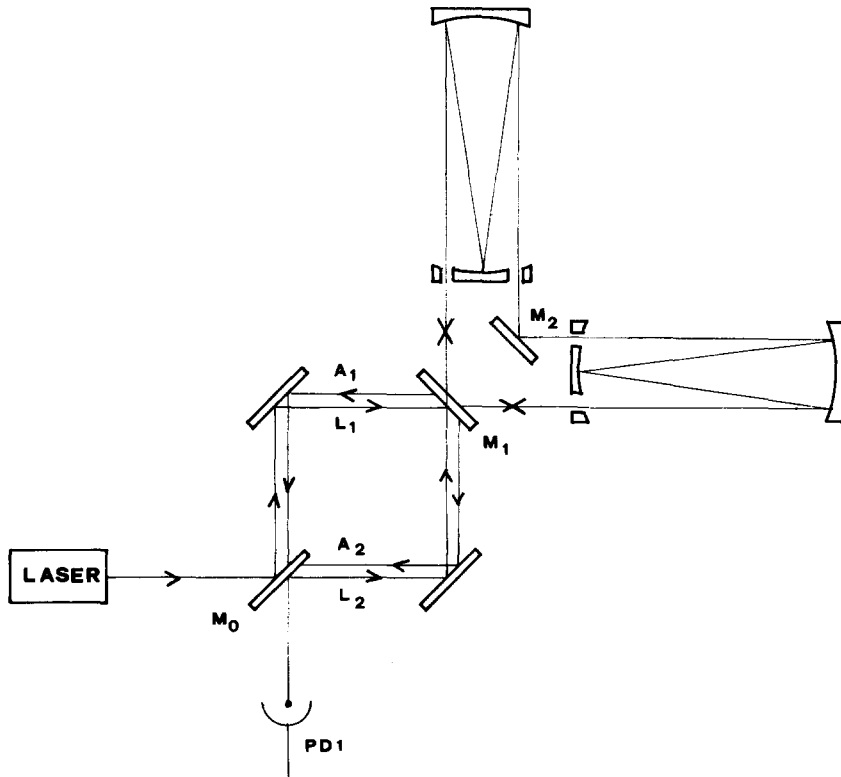
Fig. 5.4. Scheme of synchronous recycling for a DL interferometer. The laser beam enters the beam splitter M_0 and is switched, synchronously with the GW period, from one DL to the other. The photons can increase the phase shift due to the GW according to the number of switchings depending on the optical losses.

the light is switched from one DL to the other; M_2 is connected to M_1. The two beams entering the DL experience opposite phase shifts due to the GW; they then come out after having interfered on M_0 (beams A_1 and A_2) and are finally recombined by M_1 and observed by the photodiode PD1.

The reflected amplitude is easily evaluated considering the ensemble of the two cavities and of the mirrors M_0, M_3 as a generalized reflector [Vinet 1986, Vinet et al. 1988]. If the two cavities have transfer matrices G and G', then the equations for the reflected amplitude, according to fig. 5.5, are

$$A_r = i r_1 A_0 + t_1 A_2 , \qquad A_1 = t_1 A_0 + i r_1 A_2 , \qquad A_2 = i Z r_2 G G' A_1 , \tag{5.23}$$

where $Z = \exp(i\omega_0 \sum_{i=1}^{4} l_i / c)$, G, G' are the DL matrices of eq. (3.13) and $i R_i$ and t_i $(i = 1, 2)$ are the reflectivity and transmittance of mirrors M_1 and M_2.

From eq. (5.23) we can obtain the generalized reflectance,

$$S = (r_1 + \sigma_1 r_2 G G' Z)(1 + r_1 r_2 G G' Z)^{-1} , \qquad \sigma_i = r_i^2 + t_i^2 . \tag{5.24}$$

The relevant matrix elements are S_{11}, S_{21}, S_{31}, but to evaluate the effect of the resonance we can consider S_{21},

$$S_{21} = -2 t_1^2 r_2 Z \xi \, \frac{\sin^2(N\eta)}{\eta} \, \overline{y^N} b^2 (1 - r_1 r_2 Z b^2)^{-1} (1 - r_1 r_2 Z b^2 \overline{y^{2N}})^{-1} , \tag{5.25}$$

where $b = (-r)^{N-1} \rho^N x^N$, $y = \exp(i\Omega_g L / c)$, r and ρ are the reflectivities of the near and far DL mirrors, respectively.

Making $Z = +1$ and $x^N = 1$ we meet the resonant condition for the ring cavity; from eq. (5.25) it is evident that due to the synchronous recycling, the amplitude goes to zero when $\Omega_g \rightarrow 0$. A resonance occurs when $\overline{y^{2N}} = 1$, i.e., $\nu_g = \bar{\nu}_g = c/LN$. Putting $\nu_g = \bar{\nu}_g + \Delta \nu_g$, eq. (5.25) becomes

$$S_{21} \cong (-1)^{n-1} \, \frac{t_1^2 \omega \tau^*}{1 - r_1 r_2 b^2} \, \frac{1}{\pi r_1} \, \frac{1}{(1 + i \Delta \nu_g \tau^* 2\pi)} , \tag{5.26}$$
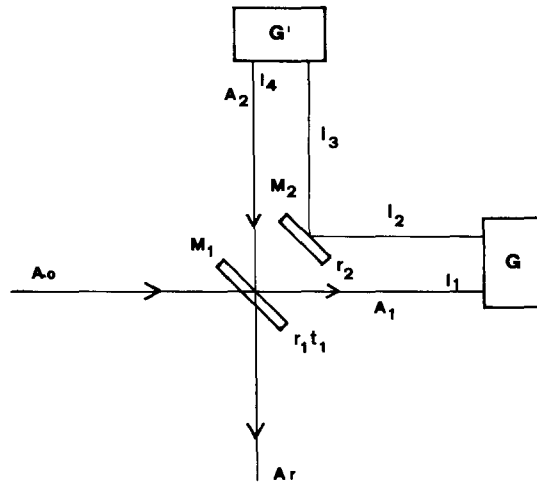
Fig. 5.5. The synchronous recycling scheme considered as a generalized reflector. A_0 and A_r are the incident and the reflected fields, respectively.

where $\tau^* = \tau_s r_1 r_2 b^2/(1 - r_1 r_2 b^2)$ is the recycling storage time. Since the resonance condition is satisfied for $\nu_g = c/4LN = \Delta\nu_0$, where $\Delta\nu_0$ is the cavity free spectral range, S_{31} is at resonance too.

As an example we may evaluate the difference between a normal DL and a SR DL, both fulfilling the condition $\nu_g = 1/(2\tau_s)$ as a function of $\Delta\nu_g/\nu_g$. From eq. (3.7) the matrix element D_{21} in the limit $\Omega_g L/c \ll 1$ becomes

$$|D_{21}| \equiv \omega/\Omega_g .$$ (5.27)

Similarly we obtain for S_{21}

$$|S_{21}| = \frac{\omega}{\Omega_g} \frac{t_1^2 B}{\pi r_1 (1 - B)^2} \left[1 + \left(\frac{\Delta\nu_g}{\nu_g} \frac{2\pi B}{1-B}\right)^2\right]^{-1/2} , \quad B = r_1 r_2 b^2 .$$ (5.28)

Equation (5.28) is valid under the condition $|\Delta\nu_g| < 1/(4\pi\tau_s)$ or $|\Delta\nu_g/\nu_g| < 1/(2\pi)$.

In fig. 5.6 $|D_{21}|\Omega_g/\omega$ and $|S_{21}|\Omega_g/\omega$ are plotted as functions of $\Delta\nu_g/\nu_g$ for $t_1^2 = 10^{-2}$ and $B = 0.99$. The maximum of $|S_{21}|\Omega_g/\omega$, having the value $t_1^2 B/[\pi r_1(1 - B)^2] = 30$, has to be compared with $|D_{21}|\Omega_g/\omega = 1$; at this gain increase one has the reduced band width (HWHM)

$$\Delta\nu_g = 2\nu_g\sqrt{3}\,\frac{1 - B}{2\pi B} \simeq \pm 5 \times 10^{-3}\,\nu_g .$$

The SR for the FP case can be evaluated from eq. (5.23) and eq. (4.3) by putting $G = F$, $r_1 = r_2$, $t_1 = t_2$, $l_1 = l_2$ and $l_3 = l_4$. The layout, shown in fig. 5.7, corresponds to a system of three coupled FP cavities. If the gravitational frequency is equal to the difference of the symmetric, ν_S, and antisymmetric, ν_A, mode frequencies, when the middle cavity is antiresonant ($Z = -1$), then the GW will be able
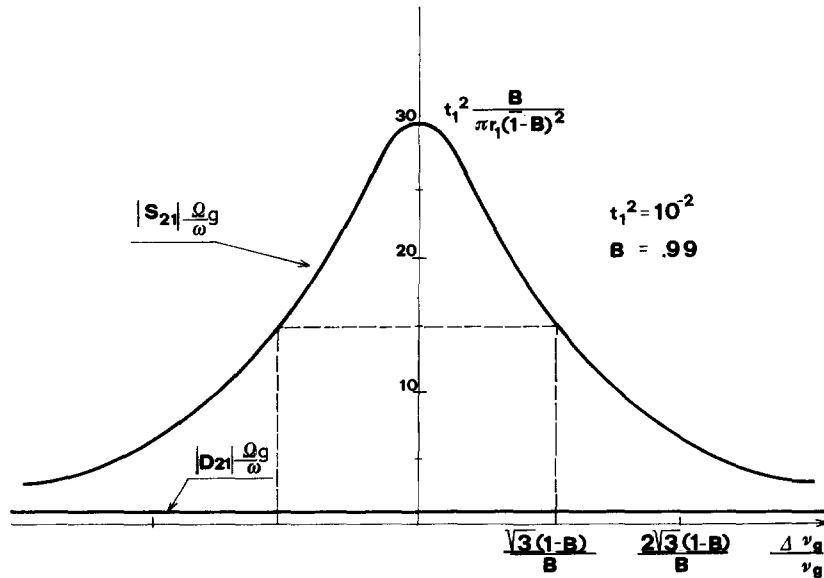
Fig. 5.6. Comparison of the side band amplitude D_{21} of a normal DL interferometer to that of a synchronous recycling DL interferometer, S_{21}. If the intensity transmittance $t_1^2 = 10^{-2}$ and the overall reflectance $B = 0.99$, then at resonance the sensitivity gain with respect to a normal DL is $\simeq 30$.
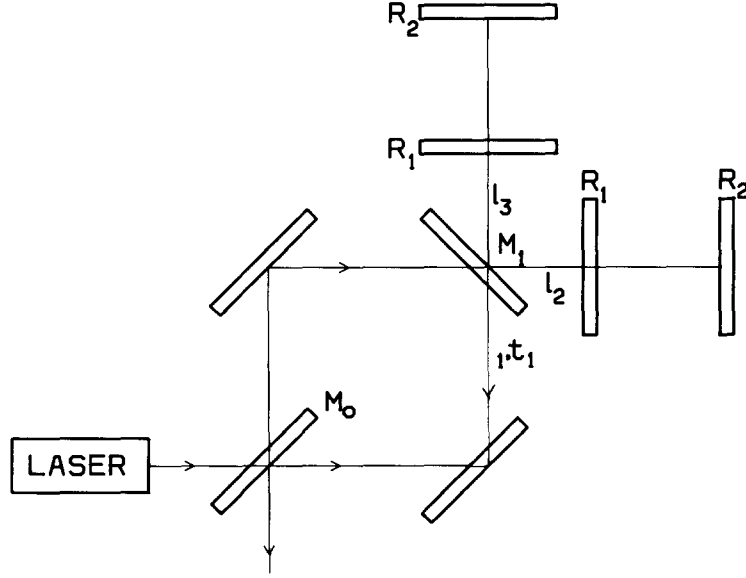
Fig. 5.7. The synchronous recycling scheme for a FP interferometer. If the GW frequency ν_g is equal to the difference of the symmetric and antisymmetric mode frequencies when the middle cavity is antiresonant, then the GW may transfer energy from one mode to the other if $\nu_g = 1/(\pi\tau_s)$.

to transfer energy from one mode to the other if $\nu_g = 1/(\pi\tau_s)$, i.e.,

$$\nu_A - \nu_S = \nu_g = 1/(\pi\tau_s) ,$$

where τ_s is defined in eq. (4.6).

The matrix element S_{31} [see eqs. (5.24), (4.4) and (2.29)] is

$$S_{31} = -2t_1^2 r_1 T_1^2 R_2^2 \xi \, \frac{\sin^2(\Omega_g L/c)}{\Omega_g L/c} \, \frac{x^2 yZ}{P(\omega)P(\omega + \Omega_g)} , \tag{5.29}$$

$$P(\omega) = (1 + R_1 R_2 \, e^{2i\omega L/c})^2 + r_1^2 Z[R_1 + (R_1^2 + T_1^2)R_2 \, e^{2i\omega L/c}]^2 . \tag{5.30}$$

Let us assume an antiresonant $(Z = -1)$ middle cavity; if $T_1^2 \ll R_1^2$ a maximum of $|S_{31}|$ is obtained when

$$\omega = \frac{c}{L}(2n + 1)\frac{\pi}{2} - \frac{\Omega_g}{2} \quad n \text{ integer} , \qquad \Omega_g = \frac{c}{L}\frac{1 - R_1 R_2}{\sqrt{R_1 R_2}} = \frac{2}{\tau_s} . \tag{5.31}$$

Due to eq. (5.29) only one of the two sidebands S_{31} and S_{21} can be made to resonate [S_{21} would require $\omega = (2n + 1)\frac{1}{2}\pi c/L + \Omega_g/2$] and this gives a S/N ratio $\sqrt{2}$ worse than in the SR for the DL case. In an analogous way to eq. (5.26) we obtain

$$S_{31} \cong \frac{t_1^2 \omega \tilde{\tau}}{1 + r_1^2 a_0} \, \frac{1}{2r_1} \, \frac{1}{1 + 2i\pi(\Delta\nu_g)\tilde{\tau}} , \tag{5.32}$$

where

$$\Delta \nu_g = \nu_g - 1/(\pi \tau_s) \,, \qquad a_0 = [R_1 - (R_1^2 + T_1^2)R_2]/(1 - R_1 R_2) \simeq -1 \,,$$

$$\tilde{\tau} = 2r_1^2 |a_0| \tau_s/(1 + r_1 r_2 a_0)$$

is the recycling time. A comparison of $|S_{31}|\Omega_g/\omega$ and $|F_{31}|\Omega_g/\omega$ [see eq. (4.4)] as a function of $\Delta\nu_g/\nu_g$ under the conditions $T_1 \gg T_2$ and $\Omega_g = 2/\tau_s$ assuming $t_1^2 = 10^{-2}$ and $r_1^2 a_0 = -0.99$, is shown in fig. 5.8.

Non-resonant recycling can be also performed with a detuned FP cavity [Vinet et al. 1988] with the purpose of increasing the cavity reflectivity. If an FP cavity is pumped with the laser frequency equal to the tuned optical frequency plus ν_g, the S/N is slightly worse than in the tuned case but the reflected intensity is closer to the incident one. This allows a larger power recycling rate and a S/N ratio closer to the SR case.

Finally in the dual recycling scheme [Meers 1988] (see fig. 5.9), a simple interferometer composed of a beamsplitter BS and far mirrors M_1, M_2 is brought to both signal and intensity resonance by means of the mirrors M_3 and M_0, respectively. The sensitivity gain is similar to that of SR but the advantage is that, unlike SR, the interferometer arms do not need to be in resonance with the GW before recycling. The tuning of the sideband to the GW frequency is done by moving the mirror M_3; this operation does not change the power stored because the beam on M_3 is at the extinction point but allows the sideband amplitude to build up.
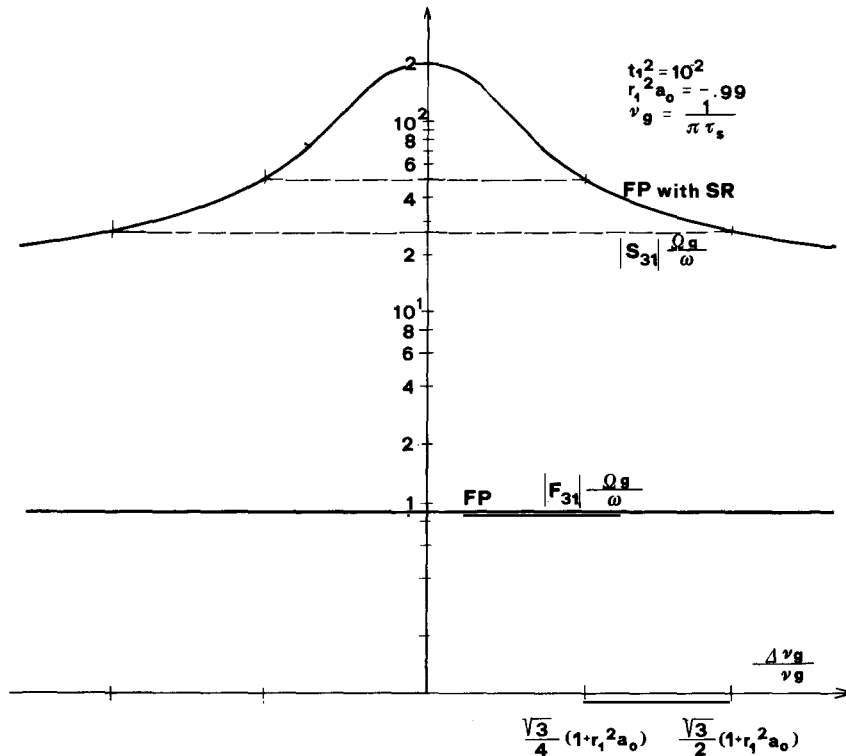
Fig. 5.8. Comparison of a normal FP and a FP with synchronous recycling. The amplitude $|F_{31}|\Omega_g/\omega$ refers to the former while $|S_{31}|\Omega_g/\omega$ refers to the latter. In both cases $\tau_s = 1/(\pi\nu_g)$. The band width (HWHM) is $\Delta\nu_g = \pm \frac{1}{4}\sqrt{3}(1 + r_1^2 a_0)\nu_g$.
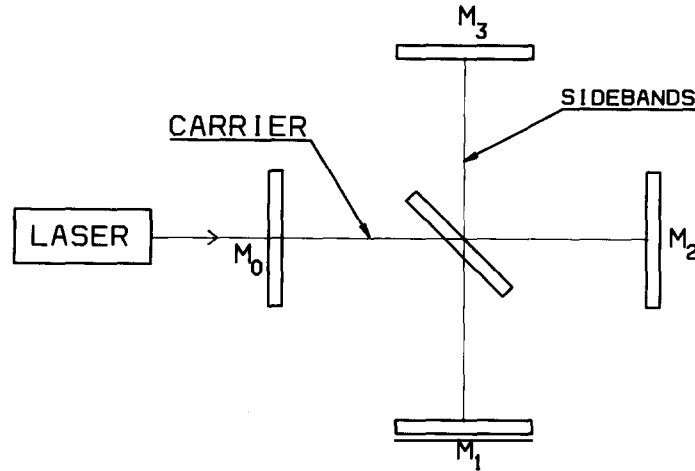
Fig. 5.9. In the dual recycling scheme both carrier and sideband are brought to resonance by moving the mirrors M_0 and M_3, respectively. The S/N ratio is similar to that obtained with synchronous recycling with the advantage that the interferometer storage time before recycling does not need to be comparable with the GW period.

6. Laser intensity noise

The laser power can be represented as

$$W(t) = W_0 + \delta W(t) ,$$

(6.1)

where W_0 is the mean power and $\delta W(t)$ is the instantaneous power fluctuation. The current I_- of eq. (5.8) refers to an ideal case where the optical elements have no losses; in a realistic case we have

$$I_- = e \, \frac{W(t)}{h\nu} \, [A - B \cos(\varphi_0 + \varphi_s)] , \qquad I_+ = e \, \frac{W(t)}{h\nu} \, [C + D \cos(\varphi_0 + \varphi_s)] ,$$

(6.2)

where $A \geq B \geq 0$ and $C \geq D \geq 0$ are coefficients close to the detection efficiency η and in general unequal, $\varphi_s = 4N\pi hL/\lambda$ and φ_0 is a given phase.

It is then evident that, since $A \neq B$, then $I_- \neq 0$ when $\varphi_0 = 0$ and this produces the noise

$$\Delta I_- = \delta W(t) \, (A - B) e/h\nu .$$

The power spectral noise $\delta W(\omega)/W_0$ typically reaches the shot noise limit $\sqrt{h\nu/W}$ for frequencies larger than $\sim 10^7$ and $\sim 10^5$ Hz for A_r [Winkler 1977, Rüdiger et al. 1981a, b] and Nd:YAG lasers, respectively.

Hence it is possible to modulate at high frequency the relative phase of the interferometer arms [Weiss 1972] by means of Pockels cells, as shown in figs. 3.5 and 3.6, and then synchronously detect the signal. This phase can be represented as

$$\varphi_M = \varepsilon_M \sin \omega_M t + \bar{\varphi}_0(t) ,$$

(6.3)

where ε_M and ω_M are the amplitude and frequency of the modulation and $\bar{\varphi}_0(t)$ is a slowly varying phase, with respect to ω_M, determined by the feedback (FB) loop in such a way as to minimize I_-. Introducing eq. (6.3) in eq. (6.2) and retaining terms up to $\sin(\omega_M t)$ we obtain

$$I_- = \frac{eW(t)}{h\nu} \left[A - B \cos(\varphi_s + \varphi_0 + \bar{\varphi}_0) J_0(\varepsilon_M) - 2B \sin(\varphi_s + \varphi_0 + \bar{\varphi}_0) J_1(\varepsilon_M) \sin(\omega_M t) \right], \qquad (6.4)$$

where J_0 and J_1 are Bessel functions. The synchronous detection gives

$$U = \frac{1}{T} \int_t^{t+T} I_-(t) \sin(\omega_M t) \, dt$$

$$= \frac{eW_0}{h\nu} \left\{ [A - B \cos(\varphi_s + \varphi_0 + \bar{\varphi}_0) J_0(\varepsilon_M)] \frac{\delta W(\omega_M)}{W_0} - B \sin(\varphi_s + \varphi_0 + \bar{\varphi}_0) J_1(\varepsilon_M) \right\}, \qquad (6.5)$$

where $\delta W(\omega_M)$ is the spectral density of the laser power noise evaluated at the frequency $\omega_M/2\pi$ and the integration time satisfies the inequality $2\pi/\omega_M \ll T \ll 1/\nu_g$.

It is possible to drive the Pockels cells with the low pass filtered signal U with the purpose of keeping
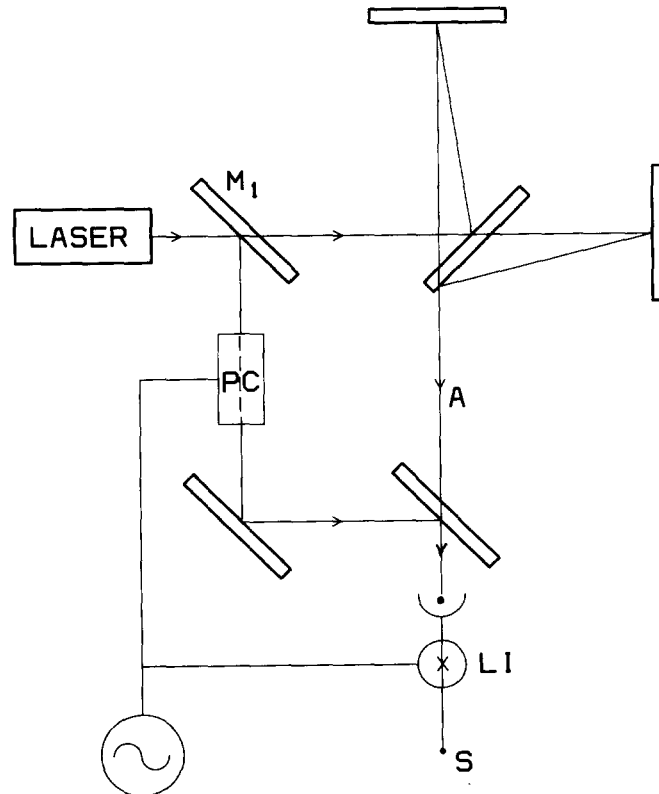
Fig. 6.1. The external modulation scheme: a small fraction of the incident power is sent through the Pockels cell PC to interfere with the outgoing amplitude A containing the GW signal. The PC is modulated at a frequency where the laser amplitude noise reaches the shot noise. Synchronous detection gives the signal S.

I_- close to extinction, hence minimizing the photon counting noise; in the limit of very large loop gain this gives $\bar{\varphi}_0 = -\varphi_0$. From this condition and from eqs. (6.4) and (6.5) it follows that the currents due to the signal (U_S) and to the noise (U_N) are

$$U_S \cong -\frac{eW_0}{h\nu}\, B\varphi_s J_1(\varepsilon_M)\,,$$

$$U_N = \left[\left(\frac{eW_0}{h\nu}\,[A - BJ_0(\varepsilon_M)]\,\frac{\delta W(\omega_M)}{W_0}\right)^2 + \frac{e^2 W_0}{h\nu}\,[A - BJ_0(\varepsilon_M)]\right]^{1/2}.$$

(6.6)

The last term on the r.h.s. of U_N is due to the photon counting noise. The best value of ε_M maximizes the S/N ratio, or equivalently the quantity $J_1(\varepsilon_M)/U_N$ [Shoemaker et al. 1987a].

It should be emphasized that in FP interferometers laser frequency fluctuations with respect to the cavity resonance frequency induce intensity fluctuations due to the narrow resonance width, and hence low frequency noise in the mirrors. To overcome this effect a precise locking of the interferometer to the laser frequency is needed.

In a large kilometric interferometer the beam size will be of the order of 10^{-1} m with the purpose of minimizing the size on the far mirror; this implies the use of Pockels cells having large aperture, impractical for being carried by the test masses. This requirement can be circumvented using an external modulation scheme, shown in fig. 6.1, in which a small fraction of the incident light is sent through a Pockels cell to interfere with the beam containing the GW signal. The Pockels cell is modulated at a frequency where the laser amplitude noise has reached the shot noise; the signal is obtained by making synchronous detection with the modulation signal. In this scheme the noise is $\simeq\sqrt{2}$ times higher [Man 1988, Paris, Orsay, Pisa, Napoli, Frascati Collab. 1988] than in the internal modulation one, but the external modulation has the advantage of bringing a net sensitivity improvement because it enhances the recycling factor.

7. The noise due to the laser linewidth

Laser frequency fluctuations produce phase noise in an interferometer with arms having unequal length. If ν_0 and $\Delta\nu$ are the laser mean frequency and the r.m.s. frequency fluctuation, respectively, then the r.m.s. phase fluctuation due to the difference in arm length ΔL is

$$\Delta\varphi \cong 2\pi\,\Delta\nu\,\Delta L/c\,.$$

(7.1)

It is then very important to avoid that rays having large ΔL interfere.

In a multipass DL interferometer the light hitting the mirrors is scattered by the reflecting coating and enters the optical path of one of the other DL beams. This phenomenon, even if the scattered beam intensity is of the order of $\varepsilon \cong 10^{-4}-10^{-5}$ of the incident one, may create a large background because the interference of the scattered beam with the main one has an amplitude proportional to $\sqrt{\varepsilon}$.

Different methods have been adopted to get rid of this phenomenon [Schilling et al. 1981, Schnupp et al. 1985]; one method [Rüdiger et al. 1981a, b] consists in "whitening" the laser light spectrum in such a way that rays having a different path length create a phase shift having an r.m.s. value equal to zero.

A more precise evaluation of this noise can be made supposing that the laser frequency fluctuations can be taken into account by means of a random phase $\phi_R(t)$ introduced into the wave function representing a monochromatic wave, i.e.,

$$\psi = A_0 \exp[i\omega t + i\phi_R(t)] , \tag{7.2}$$

where ϕ_R satisfies the correlation relation

$$\overline{\phi_R(t)\phi_R(t')} = (2\pi)^2 \, \Delta\nu^2 \, g(t - t') , \tag{7.3}$$

and $g(0) = 1$.

If the wave ψ is split by the beam splitter and then brought to interference after reflection on the far mirrors (at a distance L and $L + \Delta L$, respectively), the intensity of the interference will be

$$I \propto \sin^2[\phi_R(t - L/c) - \phi_R(t - (L + \Delta L)/c) + 2\phi_g(t)] , \quad \phi_g(t) = h\omega \, \frac{L}{c} \, \frac{\sin \Omega_g(L/c)N}{\Omega_g L/c} \, e^{i\Omega_g t} , \tag{7.4}$$

where ϕ_g [see eq. (3.10)] is the phase shift produced in the DL interferometer by the GW assumed to be periodical. Since $\Delta L/c \ll 1/\Delta\nu$ it follows that we can expand ϕ_R in a Taylor series, obtaining

$$I \propto \sin^2[\dot\phi_R(t) \, \Delta L/c + 2\phi_g(t)] . \tag{7.5}$$

We can now evaluate the noise Fourier spectrum,

$$|\phi_N(\Omega)|^2 = \left| \frac{\Delta L}{c} \int_0^T \dot\phi_R(t) \, e^{i\Omega t} \, dt \right|^2 , \tag{7.6}$$

and compare it with the signal,

$$|\phi_s(\Omega)|^2 = \left| \int_0^T \phi_g(t) \, e^{i\Omega t} \, dt \right|^2 , \tag{7.7}$$

where T is the measurement time. From eqs. (7.3) and (7.6) it follows that

$$|\phi_N(\Omega)|^2 = (\Delta L/c)^2 (2\pi)^2 \, \Delta\nu^2 \int_0^T \int_0^T g(t - t') \, e^{i\Omega(t - t')} \, dt \, dt' , \tag{7.8}$$

where the measurement time $T \gg 1/\Omega$. Putting $g(z) = \int_{-\infty}^{\infty} Q(\omega) \, e^{-i\omega z} \, d\omega$, eq. (7.8) becomes

$$|\phi_N(\Omega)|^2 = (\Delta L/c)^2 (2\pi)^2 \, \Delta\nu^2 \int_{-\infty}^{\infty} Q(\omega) \, \frac{4\sin^2(\Omega - \omega)T/2}{(\Omega - \omega)^2} \, d\omega . \tag{7.9}$$

Since the function $\sin^2(xT/2)x^2$ can be approximated with $\frac{1}{2}T\pi\delta(x)$, we obtain

$$|\phi_N(\Omega)|^2 \cong (\Delta L/c)^2 (2\pi)^2 \, \Delta \nu^2 \, \tfrac{1}{2}\pi T Q(\Omega) \,. \tag{7.10}$$

The quantity $S = 2\pi\sqrt{\tfrac{1}{2}\pi} \, \Delta \nu \, Q^{1/2}$ is measured in $Hz/\sqrt{Hz}$ and gives the linear spectral density of the laser frequency fluctuations.

Comparing eq. (7.10) with eq. (7.7) we obtain the measurability condition for h when the DL storage time is optimal [see eq. (3.9)],

$$h(\Omega_g) > \frac{\Delta L \, \Delta \nu}{\omega c} \, \Omega_g \sqrt{\tfrac{1}{2}\pi^3 Q(\Omega_g)/T} \,. \tag{7.11}$$

Equation (7.10) shows that $S(\Omega)$ can be measured by means of an imbalance of the arm length, ΔL.

The line width can be reduced by means of active systems; one method consists in operating a reference FP cavity [Drever et al. 1983, Hough et al. 1987, Shoemaker et al. 1987a] fed with a small fraction of the laser light phase modulated at the frequency ν_M by means of a Pockels cell (see fig. 3.6). If the laser frequency is tuned to one of the FP resonances the reflected light has the two sidebands at frequency $\pm \nu_M$ having amplitudes of opposite sign, giving zero output in a photodiode. If the laser frequency fluctuates the two sideband amplitudes will not cancel anymore and give a signal in the photodiode, which can be detected synchronously. The signal is proportional to the laser frequency displacement $\Delta \nu$ with respect to the FP resonance frequency. It can be fed to a laser intracavity Pockels cell (for high-frequency FB) and to a PZT (for low-frequency FB), which moves one of the laser mirrors for stabilizing the frequency. The limiting noise is the shot noise; taking it into account for a cavity having no losses, the line width becomes

$$\Delta \nu \geq \frac{1}{2\pi\tau_s} \sqrt{\frac{h\nu}{w_s t}} \,, \tag{7.12}$$

where τ_s is the reference cavity storage time, w_s is the power used in the stabilization circuit and t is the observation time.

With the purpose of further reducing the laser linewidth, the Munich group [Billing et al. 1983, Shoemaker et al. 1985] let the beam W_+ interfere (see fig. 3.7) with a small fraction of the laser beam, obtaining an output from the photodiode PD2 proportional to $\Delta \nu \, L$, where L is the total optical path length in the DL. This signal and that from the reference FP were added for improving the stabilization; in fig. 7.1 [Shoemaker et al. 1985] the upper curve represents the unstabilized laser line spectral density, the middle curve the line spectral density reduced by means of the reference FP cavity while the lower curve is the line spectral density when both reference cavity and the whole interferometer are used. The final integrated line width was $\approx 3 \, Hz$, a reduction of $\approx 10^6$ with respect to the unstabilized one.

A frequency noise level of $12.5 \, mHz/\sqrt{Hz}$ was obtained with a diode pumped Nd:YAG laser, actively frequency stabilized with respect to a reference FP cavity [Shoemaker et al. 1989].

The effects due to the laser linewidth in FP interferometers involve a more complex mechanism than in a DL interferometer; from eqs. (7.2) and (4.2) we can evaluate the reflected amplitude,

$$A_r(t) = iR_1\psi(t) + iR_1 T_1^2 \sum_{n=0}^{\infty} (-R_1 R_2)^n \psi(t - 2(n+1)L/c) \,; \tag{7.13}$$

putting
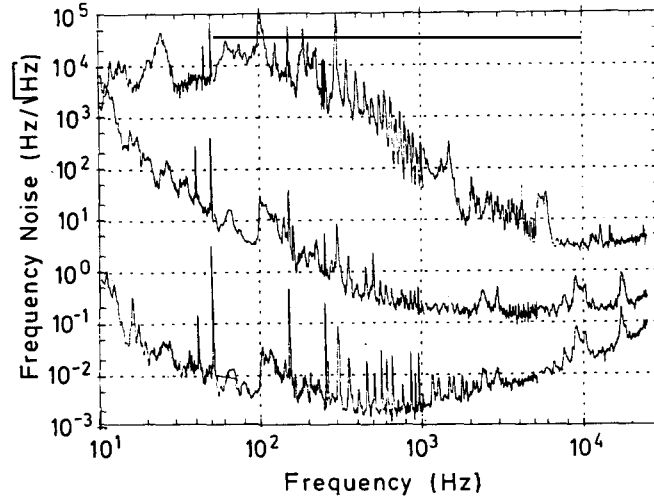
Fig. 7.1. The laser spectral line density before stabilization (from Shoemaker et al. [1985]) is shown in the upper curve; in the middle one the spectral line density after stabilization with a reference FP cavity is shown while in the lower one the spectral line density is shown after combined stabilization with the reference FP cavity and the total DL optical path.

$$\psi(t) = \int\limits_{-\infty}^{\infty} \psi(\omega)\, e^{i\omega t}\, d\omega$$

we obtain

$$A_r(t) = i \int\limits_{-\infty}^{\infty} d\omega\, \psi(\omega) \left(R_1\, e^{i\omega t} + R_2 T_1^2\, \frac{e^{i\omega(t-2L/c)}}{1 + R_1 R_2\, e^{-2i\omega L/c}} \right). \tag{7.14}$$

In an analogous way to eq. (7.4), combining the A_r from the two arms onto the beam splitter, the intensity on the photodiode is

$$I \propto \left| \int\limits_{-\infty}^{\infty} \left[\left(R_1\, e^{i\omega t} + R_2 T_1^2\, \frac{e^{i\omega(t-2L/c)}}{1 + R_1 R_2\, e^{-2i\omega L/c}} \right)_{\text{arm } 1} \right. \right.$$
$$\left. \left. + e^{i\varphi} \left(R_1\, e^{i\omega t} + R_2 T_1^2\, \frac{e^{i\omega(t-2L/c)}}{1 + R_1 R_2\, e^{-2i\omega L/c}} \right)_{\text{arm } 2} \right] \psi(\omega)\, d\omega \right|^2, \tag{7.15}$$

where φ is a given phase shift. It is evident from eq. (7.15) that unlike in the DL case, even when $(L)_{\text{arm } 1} = (L)_{\text{arm } 2}$, there is incomplete cancelation of the laser line width noise unless the mirror transmittance and losses in the two arms are equal.

In the Glasgow [Newton et al. 1986] and the Caltech [Spero 1986] FP interferometers the laser line width is stabilized by using the cavity of one of the interferometer arms as a reference (see fig. 4.3). In this case, since the stabilizing cavity is very long, the sensitivity to laser frequency changes is much higher than that of a shorter reference cavity having the same finesse.

The presence of the laser intracavity Pockels cell gives non-negligible power losses; stabilization

using extracavity phase acousto-optic modulators has been performed by Hall et al. [1977] and Camy et al. [1982]. In an experiment [Kerr et al. 1985] the use of an extracavity electro-optic modulator yielded a typical laser frequency fluctuation of $\simeq 0.01\ \text{Hz}/\sqrt{\text{Hz}}$ at 1 kHz.

8. The noise produced by the lateral beam jitter

If the beam splitter is not symmetrical between the two interferometer arms, but deviates by an angle $\delta\alpha$, then a lateral beam jitter δx will produce the phase shift [Billing et al. 1979]

$$\Delta\phi \cong 2\,\delta\alpha\,\delta x\,4\pi/\lambda\ .\tag{8.1}$$

Two methods have been adopted for reducing this type of noise: the first uses a mode cleaner [Rüdiger et al. 1981a, b, Meers 1983], while the second, a simpler one even though 30–50% of the laser power is lost, is the use of a monomode optical fiber coupler as suggested by R. Weiss of MIT. The experimental set up, shown in fig. 8.1, consists of a monomode fiber lit by a microscope objective; a $\lambda/2$ plate placed before the fiber and a linear polarizer placed behind it keep the right polarization. In fig. 8.2 [Shoemaker et al. 1985] the residual lateral beam jitter is shown as measured by a position sensitive diode: the top curve represents the laser beam jitter, the middle one the beam jitter after a mode
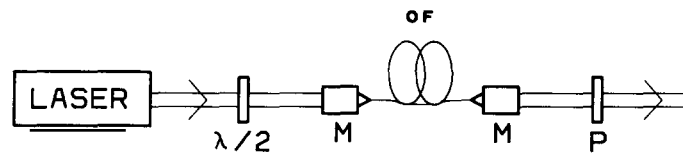
Fig. 8.1. The laser beam jitter is strongly reduced by injecting the beam in the monomode optical fiber OF. The injection is performed by means of the microscope objective M; the $\lambda/2$ plate and the polarizer P restore the plane polarization.
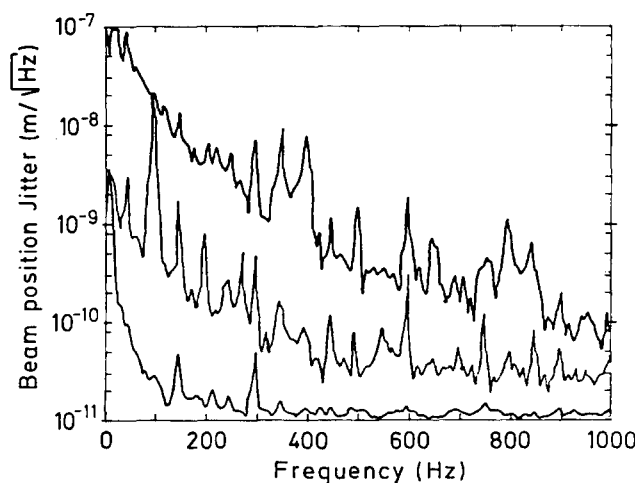
Fig. 8.2. The lateral beam jitter (from Shoemaker et al. [1985]) as measured with a position sensitive diode; the upper curve is the unfiltered laser beam, the middle one represents the beam jitter after a mode cleaner and the lower represents the jitter after a monomode optical fiber.

cleaner and the lower one the beam after the monomode fiber; a displacement of $\simeq 10^{-11}$ m/$\sqrt{\text{Hz}}$ for $\nu > 100$ Hz was obtained.

A recycling cavity would filter out the fast laser frequency and amplitude fluctuations, as well as most of the beam geometry jitter.

9. The noise due to the gas pressure fluctuations

This type of phase noise originates from the fluctuations of the refractive index in the interferometer's vacuum pipes. The laser light bounces between the mirrors of either the FP or the DL system; the number of gas molecules contained in the light pipe then fluctuates almost in a Poissonian way (there may be convective motion also), hence varying the refraction index [Brillet 1984, 1985, Hough et al. 1986].

This can be shown as follows: if V is the average light pipe volume (not the vacuum pipe diameter), the total number of gas atoms in this volume is

$$n(t) = V \sum_i \frac{\rho_i(t)}{m_i} = V \sum_i n_i(t) , \tag{9.1}$$

where ρ_i and m_i are the density and the mass of the ith gas component and $n_i(t)$ the instantaneous number of molecules of the ith gas component. The number fluctuations $\delta n_i(t)$ of the ith component satisfy the correlation relation

$$\overline{\delta n_i(t)\, \delta n_i(t')} = \overline{n}_i g_i(t - t') , \tag{9.2}$$

where $\overline{n}_i$ and g_i are the average number and the correlation function of the ith gas component, respectively, with the condition $g_i(0) = 1$.

The function g_i is a complex function of the light beam geometry; let us for the sake of simplicity, approximate the light pipe volume by a cylinder having length L and diameter D. Under this condition the correlation time is D/V_i, where V_i is the speed of the molecules of the ith gas component. The light phase shift due to the gas refraction index ε_i is (we are considering a DL)

$$\phi_{\text{G}}(t) = \frac{4\pi NL}{\lambda} \sum [\varepsilon_i(t) - 1] . \tag{9.3}$$

The phase fluctuation $\delta\phi_{\text{G}}$ is

$$\delta\phi_{\text{G}}(t) = \frac{4\pi NL}{\lambda} \sum \frac{\delta n_i(t)}{\overline{n}_i} (\overline{\varepsilon}_i - 1) . \tag{9.4}$$

In Ω space, using eq. (9.2), the noise is

$$|\delta\phi_{\text{G}}(\Omega)|^2_{\text{DL}} = \left(\frac{4\pi NL}{\lambda}\right)^2 \sum_i \int_0^T e^{i\Omega(t-t')} \int_0^T \frac{(\varepsilon_i - 1)^2 g_i(t - t')}{\overline{n}_i} \, dt \, dt' , \tag{9.5}$$

where T is the measurement time.

Assuming the simple correlation function $g(t - t') = 1 - \theta(|t - t'| - D/V_i)$, $\bar{\varepsilon}_i - 1 = \alpha_i P_i / P_{0i}$, where P_i and P_{0i} are the pipe and atmospheric partial pressure, respectively, $\bar{n}_i = P_{i\frac{1}{4}}\pi D^2 L / K\tilde{T}$ ($\tilde{T}$ is the temperature), eq. (9.5) becomes

$$|\delta\phi_G(\Omega)|^2_{\mathrm{DL}} = \left(\frac{4\pi NL}{\lambda}\right)^2 \sum_i \frac{2\sin(\Omega D/V_i)}{\Omega} T(\alpha_i P_i/P_{0i})^2 \frac{K\tilde{T}}{2NP_{i\frac{1}{4}}\pi D^2 L} .$$ (9.6)

The h measurability condition for a DL interferometer is [see eq. (7.6)]

$$\tilde{h}_{\mathrm{DL}}(\Omega) > \left[16 \sum_i \frac{\sin\Omega D/V_i}{\Omega} \left(\frac{\alpha_i}{P_{0i}}\right)^2 \frac{K\tilde{T}P_i}{N\pi D^2 L}\right]^{1/2} \frac{NL\Omega}{c \sin \Omega NL/c} .$$ (9.7)

For a FP interferometer working at optical resonance we obtain the following result [for the definitions see eqs. (4.2) and (4.5)]:

$$|\delta\phi_G(\Omega)|^2_{\mathrm{FP}} = \sum_i [\sqrt{8}\, T_1^2 R_2 \omega(L/c)(\bar{\varepsilon}_i - 1)]^2 \frac{T}{\bar{n}_i} \frac{\sin(\Omega D/V_i)}{\Omega} \frac{1}{(1 - R_1 R_2)^4} \frac{1}{1 + F' \sin^2\Omega L/c} .$$ (9.8)

Comparing eq. (9.8) with the Fourier transform [see eq. (7.7)] of eq. (4.5) we obtain the measurability condition

$$\tilde{h}_{\mathrm{FP}} \gtrsim \left(\sum_i 2 \frac{(\bar{\varepsilon}_i - 1)^2}{\bar{n}_i} \frac{\sin(\Omega D/V_i)}{\Omega}\right)^{1/2} .$$ (9.9)
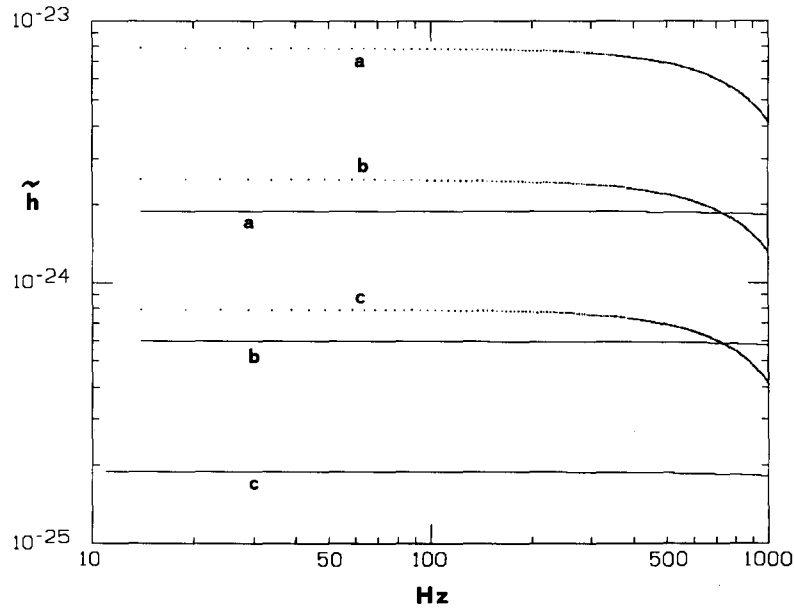
Fig. 9.1. The limits on the spectral strain amplitude for a FP interferometer having arm length $L = 3$ km, as given by the pipe vacuum fluctuations in the frequency interval $0 < \nu < 10^3$ Hz and for three pressures, a, $p = 10^{-6}$ mbar, b, $p = 10^{-7}$ mbar, c, $p = 10^{-8}$ mbar. The dotted lines are for N_2 and the solid lines are for H_2.

$\tilde{h}_{\mathrm{FP}}$ is larger than $\tilde{h}_{\mathrm{DL}}$ because the light pipe volume in the FP case is $2N$ times smaller than that of the DL.

In fig. 9.1, $\tilde{h}_{\mathrm{FP}}$ is plotted as a function of the pressure for H_2 and N_2 in the frequency interval $0 < \nu < 10^3 \, \mathrm{Hz}$.

A calculation taking into account a better approximation of the correlation function has been performed by Rüdiger [1988].

10. Thermal noise

The mass of the mirror is driven by the stochastic forces produced by thermal noise; we are considering here both the forces acting on the mirror suspensions and those producing an excitation of the mirror normal modes.

For the former case, if τ is the mirror suspension relaxation time, the r.m.s. stochastic spectral force is [Uhlenbeck and Ornstein 1930]

$$F = \sqrt{\frac{2K\tilde{T}M}{\tau}} \; \frac{\mathrm{N}}{\sqrt{\mathrm{Hz}}} \tag{10.1}$$

where M is the mirror mass, $\tilde{T}$ the temperature and K the Boltzmann constant. The thermal stochastic force $f(t)$ satisfies the correlation relation

$$\overline{f(t)f(t')} = F^2\delta(t - t') . \tag{10.2}$$

The mirror displacement $x(\Omega)$ in Ω space is evaluated using eqs. (2.17) and (10.2); in analogy with eq. (7.7) we obtain

$$|x_i(\Omega)|^2 \cong T \, \frac{2K\tilde{T}}{M\tau} \; \frac{1}{(\Omega^2 - \omega_{\mathrm{p}}^2)^2 + \Omega^2/\tau^2} , \tag{10.3}$$

where T is the measurement time and $\nu_{\mathrm{p}} = \omega_{\mathrm{p}}/2\pi$ the pendulum frequency. The pendulum thermal noise gives the following limit on the measurability of $\tilde{h}$:

$$\tilde{h} > \frac{1}{\Omega^2 L} \, \sqrt{\frac{2K\tilde{T}}{M} \sum \frac{1}{\tau}} \tag{10.4}$$

where the sum is over the mirrors.

With the purpose of evaluating the thermal noise produced by the mirror normal modes we can approximate the mirror by many harmonic oscillators each having frequency ν_i, relaxation time τ_i and equivalent mass M_i. In the proximity of the ith frequency the displacement in Ω space is sufficiently well described by eq. (10.3) replacing ω_{p} with $\omega_i = 2\pi\nu_i$. Since we consider the frequency region $\nu_{\mathrm{p}} \ll \nu \ll \nu_i$ we can approximate eq. (10.3) in the following way:

$$|x_i(\Omega)|^2 \cong T \, \frac{2K\tilde{T}}{M_i\tau_i} \frac{1}{\omega_i^4} , \tag{10.5}$$
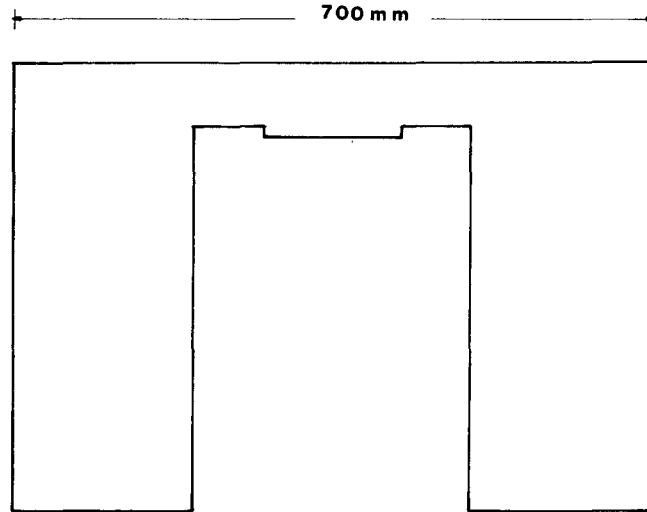
Fig. 10.1. A possible scheme of a 350 kg quartz mirror to be used in a 3 km FP interferometer for GW detection. A distortion $<\lambda/8$ is expected to be given by the 80 mm thick quartz window. The lowest-frequency mode (bell mode) at 1900 Hz it is not expected to give longitudinal mirror oscillations. The first longitudinal mode is at 2500 Hz.

with $\omega_i \tau_i = Q_i$. The $\tilde{h}$ measurability condition is

$$\tilde{h} > \frac{1}{L} \sqrt{2K\tilde{T} \sum \frac{1}{M_i Q_i \omega_i^3}} \,, \tag{10.6}$$

where the sum is over the mirrors and over the longitudinal modes.
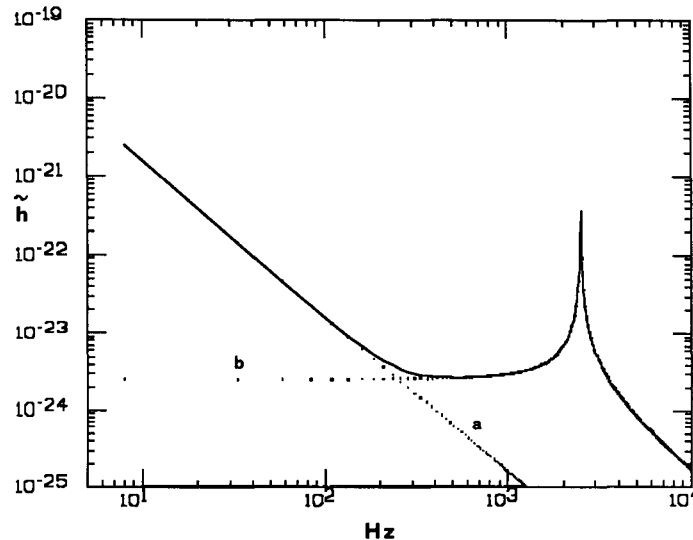
Fig. 10.2. The spectral strain amplitude sensitivity due to the mirror (see fig. 10.1) thermal noise in the frequency range $10 < \nu < 10^4$ Hz for interferometer arm length $L = 3$ km. Curve a represents the contribution from the mirror pendulum motion with $M = 300$ kg and $Q = 10^6$, while curve b represents the contribution to the thermal noise due to the mirror longitudinal normal modes. In b only the contribution from the first normal mode at 2500 Hz, having assumed an oscillator equivalent mass of $M_1 = 150$ kg and $Q_1 = 10^6$, is taken into account.

Assuming Q_i to be invariant under a scale transformation changing the mirror dimensions, it follows that eq. (10.6) is invariant too. This is not true anymore for eq. (10.4), which shows that an increase in the mass M reduces the thermal noise. At low frequency it then seems convenient to use mirrors weighing several 100 kg if possible.

The scheme of a possible 350 kg quartz mirror to be used in the 3 km FP interferometer of the VIRGO project [Pisa, Napoli, Frascati, Orsay, Paris Collab. 1987, Paris, Orsay, Pisa, Napoli, Frascati Collab. 1988] is shown in fig. 10.1; the quartz window is expected to give $<\lambda/8$ error to the wave front. The lowest frequency mode at $\simeq 1990$ Hz (bell mode), due to the cylinder hole, does not give a longitudinal oscillation to the mirror; the first longitudinal mode is at 2500 Hz.

The values of $\tilde{h}$ given for this kind of mirror considering that four mirrors will be mounted in the interferometer and assuming $Q = \tilde{\omega}_p \tau = 10^6$ in eq. (10.5), $Q_1 = 10^6$ in eq. (10.7), $L = 3$ km and $\tilde{T} = 300$ K, are shown in fig. 10.2 in the frequency interval $10 < \nu < 10^4$ Hz.

11. Seismic noise

Seismic noise is the dominant source of displacement of the mirror suspension points. The r.m.s. spectral displacement can be sufficiently well approximated by the formula

$$x_T = a/\nu^2 \text{ m}/\sqrt{\text{Hz}} ,\tag{11.1}$$

where $a \cong 10^{-9}$ at a depth of $\sim 10^3$ m up to $a \cong 10^{-6}$ at the Earth's surface in a relatively quiet place. Extensive measurements of the Earth's strain spectrum from 10^{-8} to 10^2 Hz using a laser interferometer have been performed by Berger and Levine [1974].

Experimental evidence of this type of noise [see eq. (2.13)] is clearly shown in fig. 11.1 [Shoemaker et al. 1985]; from these data the value $a \cong 10^{-7}$ can be inferred. Active systems have been used to reduce seismic noise both in the vertical [Faller and Rinker 1979, Saulson 1984a, b] and horizontal directions [Robertson et al. 1982, Giazotto et al. 1986a, b]. Three-dimensional pneumatic active systems have been developed by Lorenzini [1972].
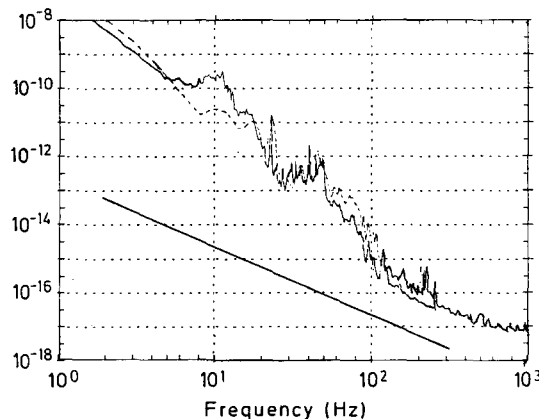
Fig. 11.1. Displacement noise of the Munich [Shoemaker et al. 1985] DL interferometer. Assuming the mirror to be suspended by a 1 m long wire, it follows that the suspension point is approximately shaken by a spectral seismic noise displacement $\Delta x \simeq 10^{-7}/\nu^2$ m/$\sqrt{\text{Hz}}$.

The basic idea consists in using an accelerometer to sense the displacement of the suspended mass, then using the accelerometer signal to create a force on the mass in such a way that the signal becomes null. In the experiment of Faller and Rinker, a sensor measured the elongation Δy of a vertical spring with respect to a fixed reference point y_0. This signal was fed to a transducer displacing the suspension point y_1 by an amount $y_0 + \alpha \Delta y$, where α is the amplification. This gives the spring motion equation

$$y = \frac{y_0 \omega_0^2 (1 - \alpha)}{-\Omega^2 + i\Omega/\tau + \omega_0^2 (1 - \alpha)} , \tag{11.2}$$

where $\nu_0 = \omega_0/2\pi$ is the open loop resonance frequency. From eq. (11.2) it follows that the equivalent spring length increases by the factor $1/(1 - \alpha)$; about 1 km was obtained.

In Saulson's experiment the acceleration of the end point of a horizontal beam was measured in the vertical direction by means of an accelerometer; the amplified signal was fed to a force transducer acting on the beam end point. In the limit of ideal accelerometer the effect of this loop was to increase the beam mass; the open loop 4.5 Hz resonance frequency was reduced, when the loop was closed, to 4×10^{-2} Hz.

The layout of the horizontal direction isolation experiment of Robertson et al. is shown in fig. 11.2. The relative displacement of the test mass with respect to the suspension point was measured by means of condensers connected to a reference arm correcting for the effects due to the ground rotations. Neglecting the ground rotations the equation of motion for the test mass in the horizontal x direction is

$$\ddot{x} + \dot{x}/\tau + (g/l)x = x_s g/l , \tag{11.3}$$
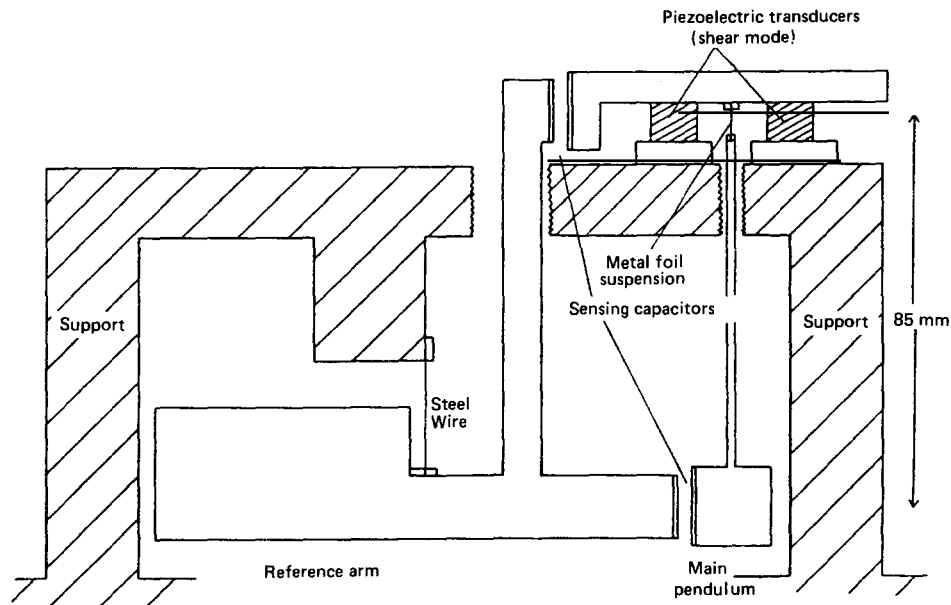
Fig. 11.2. The layout of an active horizontal direction seismic isolation experiment (from Robertson et al. [1982]). The relative displacement of the test mass with respect to the suspension point was measured by means of a capacitive transducer and fed back to a PZT acting on the pendulum suspension point. A reference arm corrected for the effects due to ground rotations. With this experiment an amplification $A = 60$ was obtained and the pendulum length was increased up to $\simeq 5$ m.

where τ is the relaxation time, x the mass coordinate, x_s is the horizontal displacement of the pendulum attachment point, g is the acceleration of gravity and l the pendulum length.

Since the capacitor c senses $x - x_s$, the PZT transducer displacement is

$$x_s = (\alpha + \beta \int dt)(x - x_s) + x_T ,$$ (11.4)

where x_T is the horizontal ground seismic noise [see eq. (11.1)] and the integral creates "cool" damping [Forward 1978].

From eqs. (11.3) and (11.4) it follows that

$$x = \left(\frac{g}{l} \frac{x_T}{1+\alpha} \right) \Big/ \left[-\Omega^2 + i\Omega \left(\frac{1}{\tau} + \frac{\beta}{1+\alpha} \right) - \left(\frac{\beta}{\tau} - \frac{g}{l} \right) \frac{1}{1+\alpha} \right] .$$ (11.5)

From eq. (11.5) it follows that the effect of α in the FB is to make the pendulum virtual length equal to $l(1 + \alpha)$ and that of β is to introduce a new damping with relaxation time $(1 + \alpha)/\beta$. With a 0.47 kg mass and $l = 85$ mm, $\alpha = 60$ on a band width of 30 Hz was obtained.

In the experiment of Giazotto et al., shown in fig. 11.3, in which a large mass (100 kg) and an interferometric sensor were used, a 1 m pendulum was brought to a virtual length of 1600 m at 10 Hz by
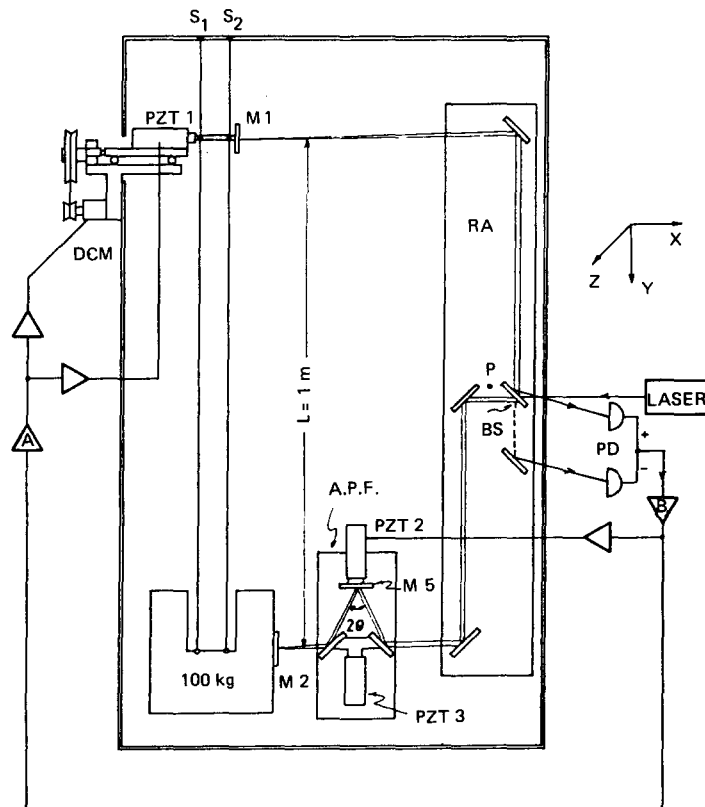
Fig. 11.3. Schematic diagram of the interferometric pendulum for seismic noise reduction (from Giazotto et al. [1986b]). The relative displacement of the 100 kg test mass with respect to the suspension point was measured interferometrically. The 1 m pendulum was brought to a length of 1600 m.

means of an analog phase follower [Campani et al. 1986], whose purpose was to transform in real time the interferometer output, proportional to $\sin \varphi$ (φ is the interferometer phase shift), to a signal proportional to φ suitable to be used as a FB signal. The pendulum suspension point was displaced by both a PZT and a DC motor; the use of the latter was crucial for obtaining high FB amplification.

A method for actively reducing the damping produced by the flexure of the pendulum suspension wire at its attachment point has been proposed and tested by Faller et al. [1987]; they obtained an increase of 5.6 in the damping time and a lowering of the pendulum resonance frequency.

The use of active seismic isolation schemes is strongly limited by the difficulty of making multiple three-dimensional (3D) systems; this necessity is dictated by the fact that a non-isolated degree of freedom reintroduces the seismic noise even if the other degrees of freedom are isolated. For this reason passive schemes have been adopted, able to isolate in the vertical direction as well [Giazotto 1987, Shoemaker et al. 1987a].

The basic idea is to use a multiple-stage pendulum with the masses supported by springs. It can be shown that the frictionless transfer functions for both the vertical and horizontal directions can be brought to the following canonical form:

$$F = \prod_{n=1}^{N} \omega_n^2/(-\Omega^2 + \omega_n^2) , \tag{11.6}$$

where F is the transfer function, $\nu_n = \omega_n/2\pi$ is the nth mode frequency and N is the number of masses. Above the resonances $F \propto \Omega^{-2N}$, but the presence of friction and nonlinearities can give a slower decrease with frequency as well as coordinate mixing.

In the interferometric antennas aiming to reach very low frequency ($\nu \geq 10$ Hz) seismic isolation requires a very careful design with the purpose of avoiding mechanical resonances falling into the interval $10 \leq \nu \leq 100$ Hz; these are produced mainly by the springs' rocking and normal modes.

To this end a 3D seven-stage seismic attenuator (see fig. 11.4) equipped with gas springs [Del Fabbro et al. 1988a] has been built by the Pisa group [Del Fabbro et al. 1987]; this attenuator is able to levitate a 400 kg test mass. The gas springs, shown in fig. 11.5, are able to levitate 10^3 kg with a rigidity of 3.4×10^4 N/m when used with four bellows and 5×10^2 kg with a rigidity of 2×10^4 N/m when used with two bellows; the normal modes of the bellows are damped by means of dry mechanical adsorbers. The rocking modes are kept at very low frequency (1 Hz) by making the wire attachment points very close to each other (5 mm).

The transfer functions for the vertical and horizontal directions [Del Fabbro et al. 1988b] in the frequency interval $10 \leq \nu \leq 68$ Hz are shown in fig. 11.6. The absolute test mass noise was measured with a dip-coil accelerometer having a sensitivity of 10^{-13} m/$\sqrt{\text{Hz}}$; fig. 11.7 shows the test mass displacement in the frequency interval $0 \leq \nu \leq 10$ Hz together with the exciting seismic noise. Taking the ratio between these two spectra, the transfer function measured for $0 \leq \nu \leq 10$ Hz shows that there is a $\sim 10^{-2}$ vertical to horizontal coupling [Del Fabbro et al. 1988c].

The general problem of cool damping [Forward 1978, Kuroda et al. 1982] of the pendulum normal modes has been solved by means of both electromagnetic or electrostatic force actuators. In the Munich, Glasgow and Caltech interferometers use was made of magnet and coils, while in the MIT interferometer electrostatic transducers were used.

The basic layout of an electromagnetic damping scheme [Shoemaker 1987] is shown in fig. 11.8. The mass position is read by means of a position sensitive diode PSD illuminated by a LED. After differentiating the signal with respect to time, which produces an effective viscous force, it is applied to coil C producing a force on magnet M connected to the test mass.
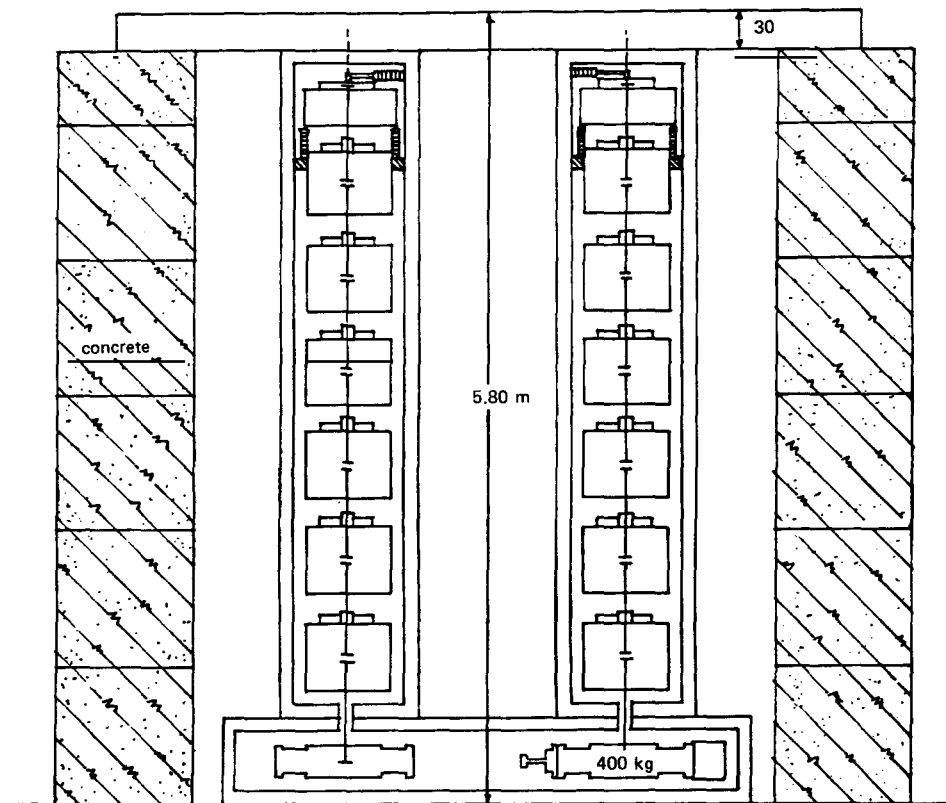
Fig. 11.4. Schematic diagram of the seismic noise attenuator (from Del Fabbro et al. [1988b]). The two attenuators, composed of a 7-fold three-dimensional harmonic oscillator, are able to give isolation in the vertical direction as well. The 400 kg test masses contained in the vacuum chamber are also shown. This device is able to attenuate the seismic noise in the vertical direction by a factor of $\leq 2 \times 10^{-8}$ at 10 Hz.
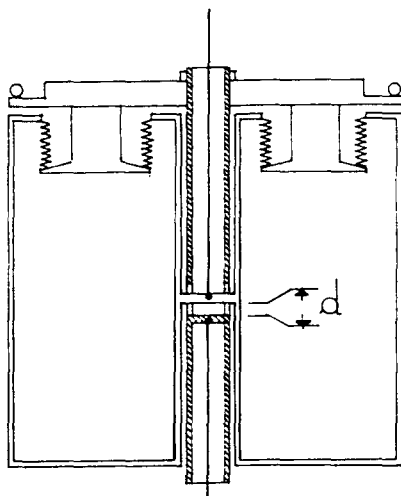
Fig. 11.5. The schematic diagram of a gas spring (from Del Fabbro et al. [1988a]). The gas pressure pushes the bellow piston, which levitates the load attached to the lower wire. A rigidity of 34×10^3 N/m with four bellows and of 20×10^3 N/m with two bellows was obtained.
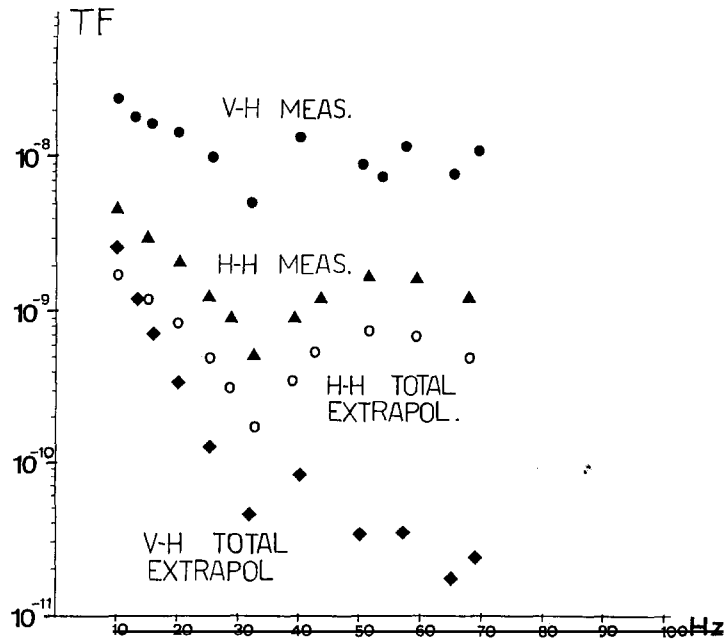
Fig. 11.6. The vertical and horizontal TF for the seismic noise attenuator of fig. 11.4 (from Del Fabbro et al. [1988b]) in the frequency interval $10 \leq \nu \leq 68$ Hz. The excitations were applied to the second stage in the chain; hence these plots give upper limits. At 10 Hz the vertical–horizontal (V–H) TF was $<2.8 \times 10^{-8}$, while the horizontal–horizontal (H–H) TF was $<5 \times 10^{-9}$. An extrapolation to the suspension point excitation gives at 10 Hz, V–H $\leq 3 \times 10^{-9}$ and H–H $< 2 \times 10^{-9}$.

A low-pass filter (LPF) prevents the damping system to reintroduce seismic noise. This problem, which is easily solved for interferometers designed to work at high frequency ($\nu \geq 200$ Hz), becomes crucial for those aimed to work at low frequency. In the Pisa attenuator, having normal modes for $\nu \leq 6$ Hz, it is necessary to have an LPF cutting the FB at 10 Hz not giving instabilities; this is a complex problem to be solved. A six-dimensional damping system using PSD has been built to reduce the amplitude of the 0.24 Hz pendulum mode of the Pisa attenuator; an absolute displacement of the test mass of $\simeq 3$ μm was obtained [Bradaschia et al. 1989]. The use of accelerometers instead of PSD could prevent the injection of seismic noise.

Seismic noise affects the interferometer phase also by means of the interaction of the mirror scattered light with the vacuum pipe walls [Billing et al. 1983]: the scattered light is reflected by the pipe walls and then reenters the main beam by means of a second scattering process. Since the pipe walls are vibrating, due to the seismic noise, they change the phase of the scattered beam; the interference of the scattered beam with the main one then reintroduces the seismic noise despite the seismic isolation of the mirrors. The use of diaphragms in the vacuum pipe could prevent the scattered light which hits the pipe walls to reenter the main optical path. A thorough evaluation of the effects of light scattering and a study of baffle configurations inside the vacuum pipe has been made by Thorne [1989]; the use of seismically isolated diaphragms for low-frequency GW detectors has been proposed by Giazotto [1988a].

The effects of the Newtonian forces produced by moving objects have been evaluated by Saulson [1984a, b] and found to be negligible with respect to other type of noise at the expected sensitivity of the new generation of antennas.
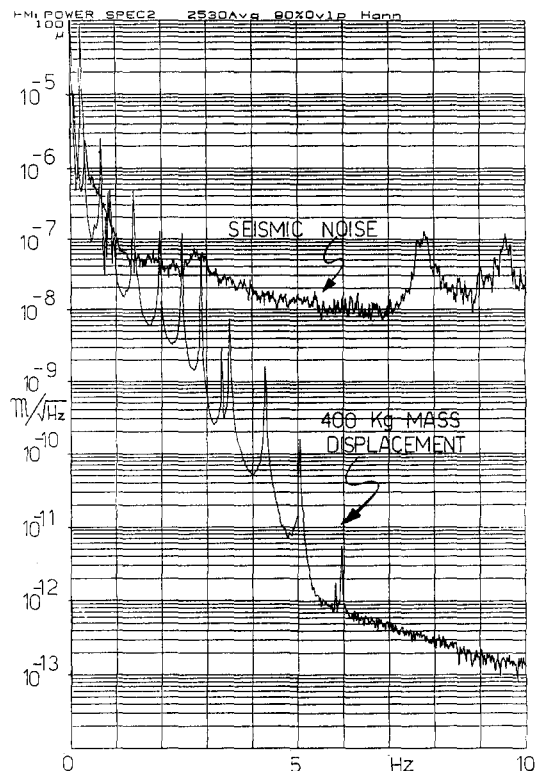
Fig. 11.7. The displacement spectrum of the 400 kg test mass of the apparatus shown in fig. 11.4 in the frequency interval $0 \le \nu \le 10\,\mathrm{Hz}$ (from Del Fabbro et al. [1988c]). Despite the fact that the accelerometer sensitivity is maximal in the horizontal direction, many vertical normal mode peaks are visible; a 10^{-2} mixing vertical–horizontal was measured, showing the necessity to have the vertical isolation as good as the horizontal one.
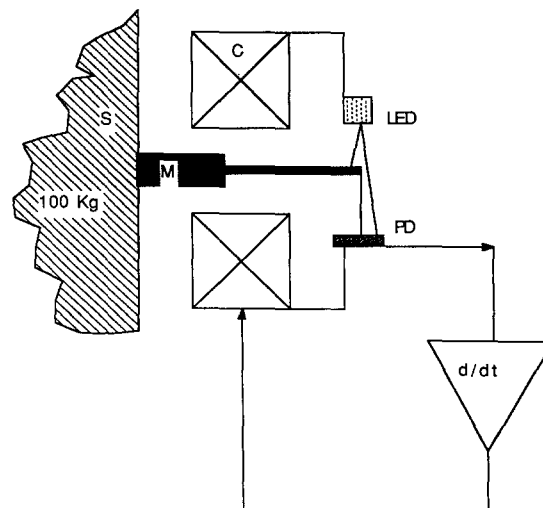
Fig. 11.8. Schematic diagram of a shadow meter damping system: the displacement of the mass S is measured by photodiode PD; the time differential of this signal is applied to coil C, which creates a viscous force on magnet M.

12. Effects due to the radiation pressure on the mirrors

As has been shown in section 5, radiation pressure creates a differential motion of the interferometer mirrors and this effect can be easily evaluated. Since $\sqrt{n} = \sqrt{Wt/h\nu}$ is the fluctuation of the number of photons impinging on the mirrors in a time t, the momentum fluctuation is $\Delta P = (h\nu/c)\sqrt{Wt/h\nu}$, from which it follows that the rms differential spectral force is given by $\Delta \tilde{F} = (h\nu/c)\sqrt{W/h\nu}$.

In a DL system having $2N$ beams, these force fluctuations are coherently added and the measurability condition for $\tilde{h}$ is [see eq. (2.9)]

$$\tilde{h}_{\mathrm{DL}} > \frac{1}{M\Omega^2 L} \frac{2N}{c} \sqrt{Wh\nu} \, , \tag{12.1}$$

where W is the incident power.

In a FP cavity whose input and far mirrors have amplitude transmittance T_0 and T_1, respectively, the

intracavity power at optical resonance is

$$W_{in} = WT_0^2 F^2/\pi^2 ,$$ (12.2)

where $F \cong \pi\sqrt{R_0 R_1}/(1 - R_0 R_1)$ is the cavity "finesse". If $T_0 \gg T_1$ eq. (12.2) becomes

$$W_{in} \simeq W(2/\pi)F .$$ (12.3)

The fluctuations of the incident power will be coherently transmitted to the mirror for frequencies smaller than $1/\tau_s$; in this case the measurability condition for $\tilde{h}$ is

$$\tilde{h}_{FP} > \frac{1}{M\Omega^2 L} \frac{2F}{\pi c} \sqrt{Wh\nu} .$$ (12.4)

Assuming $\Omega = 60 \, \text{rad/s}$, $M = 4 \times 10^2 \, \text{kg}$, $L = 3 \times 10^3 \, \text{m}$, $h\nu \simeq 10^{-19} \, \text{J}$, $(2/\pi)F \simeq 2N \simeq 30$ it follows from eqs. (12.1) and (12.4) that

$$\tilde{h}_{DL} = \tilde{h}_{FP} \simeq 2 \times 10^{-26} \sqrt{W} \, \text{Hz}^{-1/2} .$$ (12.5)

Equation (12.5) shows that kilowatts of power can be used before reaching the photon counting limit of eq. (3.2).

In a FP interferometer the radiation pressure can create multistability; this phenomenon was experimentally observed in a cavity composed of a fixed mirror and a 60 mg moving suspended mirror [Dorsel et al. 1983]. When the intracavity power reached 100 mW a bistable response was obtained.

This effect has been theoretically investigated by Deruelle and Tourrenc [1984], Tourrenc and Deruelle [1985] and by Meystre et al. [1985]. Bistability in a three-mirror system was investigated by Meystre et al. [1985]. Following the approach of Aguirregabiria and Bel [1987] we consider a pendular cavity as shown in fig. 12.1. The reflection and transmittance coefficients of mirror M_1 are $R = (\cos \theta) e^{-i\mu}$ and $T = i(\sin \theta) e^{-i\mu}$, respectively; P is the incident light power, $D_s + x(t)$ the mirror separation and $\phi_A = \sqrt{P} \exp[-i(2\pi/\lambda)(ct + \alpha)]$ the incident light field. The light field $\phi(t)$ on mirror M_2 is

$$\phi(t) = T\phi_A\{t - [D_s + x(t)]/c\} - R\phi(\hat{t}) ,$$ (12.6)

where the retarded time $\hat{t}$ is defined as

$$c(t - \hat{t}) = D_s + x(t) + x(\hat{t}) .$$ (12.7)

Neglecting the effects of the delay, the equation of motion of mirror M_2 is

$$\ddot{x} + (\Omega/Q)\dot{x} = -\Omega^2 x + 2|\phi|^2/Mc$$

$$= -\Omega^2 x + \frac{2P}{Mc} \frac{\sin^2\theta}{1 + \cos^2\theta + 2\cos\theta \, [(4\pi/\lambda)(D_s + x) - \mu]} ,$$ (12.8)

where M is the mass of mirror M_2, Ω the pendulum angular frequency and Q the mechanical quality
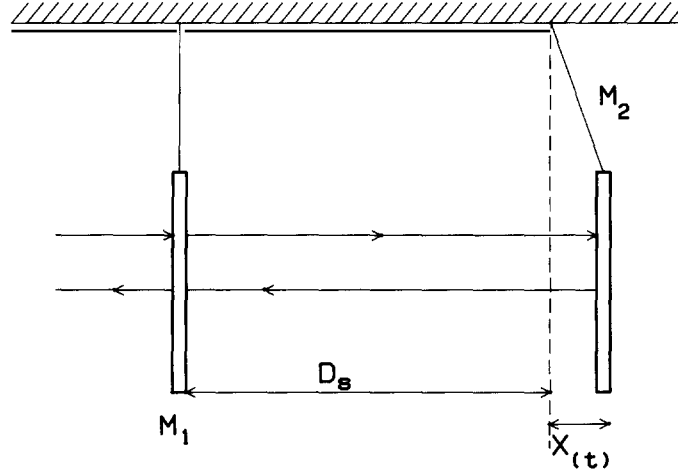
Fig. 12.1. Radiation pressure displaces mirror M_2 from its equilibrium position. $x(t)$ is then a multistable function of the radiation pressure.

factor. The relative maxima of the r.h.s. of eq. (12.8), to a good approximation, occur when

$$x = (\lambda/4\pi)[(2n + 1)\pi + \mu] - D_s = x_n \quad (n = 0, \pm 1, \pm 2, \ldots),$$

as shown in fig. 12.2 The peak heights $J = (4P/Mc\Omega^2)(F/\pi)$, where F is the finesse, can be increased more and more in such a way that a new peak crosses the $y = 0$ axis and consequently a new stability point emerges $(\partial y/\partial x < 0)$.

The delay can be taken into account writing eq. (12.6) in the following way [Aguirregabiria and Bel 1987]:

$$f(t) = 1 + (\cos \theta)\, e^{ix_s}\, e^{i[x(t-r_1)-X_s]}f(t - r_1),$$ (12.9)

where r_1 is the time needed by the light to make a round trip in the cavity ending at time t, x_s is the equilibrium point and

$$f(t) = -\frac{i\phi(t)}{\sqrt{P}\sin\theta}\, \exp\{i[(2\pi/\lambda)(ct - D_s - x + \alpha) + \sigma]\}.$$ (12.10)

Iteration of eq. (12.9) gives

$$f = 1 + \sum_{n-1}^{\infty} (\cos\theta\, e^{ix_s})^n \exp\left(i \sum_{J=1}^{n} (x_{(J)} - x_s)\right),$$ (12.11)

where $x_{(J)} \simeq x(t - Jr)$ and $r = 2D_s/c$.

The equation of motion of the pendulum becomes

$$\ddot{x} + (\Omega/Q)\dot{x} = -\Omega^2 x + (2P/Mc)\sin^2\theta\, |f|^2.$$ (12.12)

The dominant reduction of the hereditary equation of motion, evaluated up to second order in the
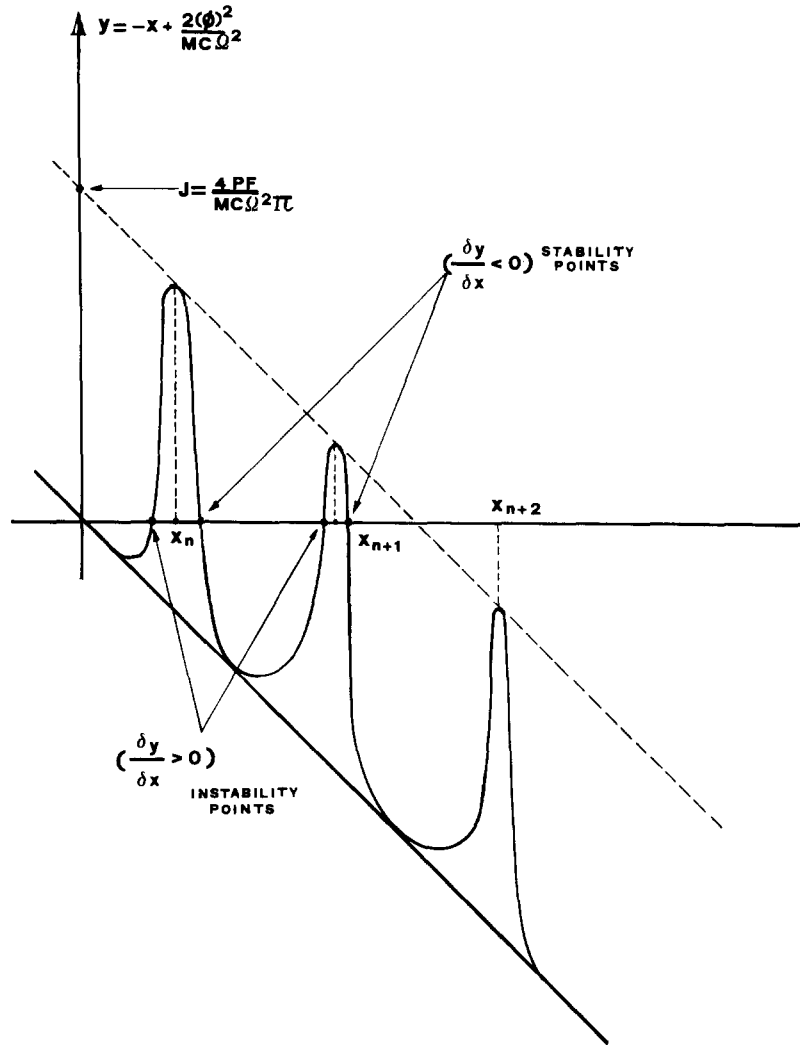
Fig. 12.2. Plot of the r.h.s. of eq. (12.8); if the laser power P increases, the peak at x_{n+2} may cross the $y = 0$ axis, thus creating a new stability point $(\partial y/\partial x < 0)$.

displacement $x(t) - x_s$, can be put in the form [Bel et al. 1988]

$$\ddot{Y} + K\dot{Y} + \bar{\Omega}^2 x = 0 ,$$

$$K = \left[\left(\frac{1}{Q} - \frac{8ry_s}{\beta\theta^2(1+y_s^2)^3}\right) - \frac{8r(1-5y_s^2)}{\beta\theta^2(1+y_s^2)^4} \, y\right]\Omega ,$$

(12.13)

$$\bar{\Omega}^2 = \left[\left(1 + \frac{2y_s}{\beta(1+y_s^2)^2}\right) + \frac{1-3y_s^2}{\beta(1+y_s^2)^3} \, y\right]\Omega^2 ,$$

where $y_s = 2x_s/\theta^2$, $\beta = \theta^4 MC/16P$ and $Y = 2[x(t) - x_s]/\theta^2$. The effect of the delay is then to add a new "friction" term [Deruelle and Tourenc 1984].

To demonstrate the presence of chaos we write eq. (12.12) putting $z = x(t) - x_s$,

$$\ddot{z} + (\Omega/Q)\dot{z} + z = (|g|^2 + 2\,\mathrm{Re}\ g)S,$$ (12.14)

where

$$\varepsilon = (4\pi/\lambda)(D_s + x_s) - \mu - (2n + 1)\pi, \qquad S = \frac{2P}{Mc}\ \frac{\sin^2\theta}{1 + \cos^2\theta - 2\cos\theta\cos\varepsilon},$$

$$g = f/f_0 - 1 = \cos\theta\ e^{i\varepsilon}\{e^{i[(4\pi/\lambda)z(\hat{t})]}[g(\hat{t}) + 1] - 1\}, \qquad c(t - \hat{t}) = 2(D_s + x_s) + z + z(\hat{t}).$$ (12.15)

Linearizing and then iterating eq. (12.15), eq. (12.14) becomes [Aguirregabiria and Bel 1987]

$$\ddot{z} + \frac{\Omega}{Q}\,\dot{z} + r^2 z = -\frac{8\pi}{\lambda}\ S \sum_{k=1}^{\infty} \mathrm{Im}(\cos\theta\ e^{i\varepsilon}z(\hat{t}_k)),$$ (12.16)

where $(\hat{t}_k)$ is the retarded time iterated k times. Putting

$$z = e^{\lambda t},$$ (12.17)

we obtain the characteristic equation

$$\lambda^2 + \frac{\Omega}{Q}\,\lambda + r^2 = -\frac{8\pi}{\lambda}\ S\cos\theta\sin\varepsilon\ \frac{1}{R}\ \frac{1}{1 + R^{-1}[(e^{\lambda r} - 1) + (e^{-\lambda r} - 1)\cos^2\theta]},$$ (12.18)

where $R = 1 + \cos^2\theta - 2\cos\theta\cos\varepsilon$ and $r = 2(D_s + x_s)/c$. Due to eq. (12.17) instability occurs when $\mathrm{Re}\ \lambda > 0$; hence the point $\mathrm{Re}\ \lambda = 0$ is the bifurcation point. The power P for any r, giving rise to instability, has also been evaluated.

In the VIRGO project [Pisa, Napoli, Frascati, Orsay, Paris Collab. 1987, Paris, Orsay, Pisa, Napoli, Frascati Collab. 1988] having arm length of 3 km, $\lambda = 1\,\mu\mathrm{m}$, power 500 W, mirror mass 400 kg, finesse $F = 30$ and pendular mechanical quality factor $Q \simeq 10^6$, the retarded effects [Tourrenc, private communication] give the unstable equation of motion for the mirror

$$Y = A\exp(2 \times 10^{-3}\,t)\sin(6t + \phi).$$ (12.19)

This instability seems to be easily corrected for by means of active feedback of the mirror damping.

13. Cosmic ray background

The interaction of particles with matter excites oscillation modes which can be experimentally detected. In an experiment [Beron and Hofstadter 1969] the modes of a piezoelectric disc have been excited by an electron beam containing 10^4–10^6 particle per pulse of 1 μs duration.

In a subsequent experiment [Grassi Strini et al. 1980] the interaction of 30 MeV protons with an Al

rod 0.2 m long and 3×10^{-2} m diameter was studied. The effect was the excitation of the rod's fundamental longitudinal mode with an amplitude

$$\xi = \frac{\alpha}{C_V} \frac{2WL}{\pi M} \cos \pi x / L \ , \tag{13.1}$$

where L is the rod length, W the energy lost by the hitting particles, α the rod thermal linear expansion coefficient, C_V the specific heat at constant volume, M the mass of the rod and x the distance from the center at which the particles cross the rod. Theoretical calculations [Allega and Cabibbo 1983, Bernard et al. 1984] have been performed giving good agreement with eq. (13.1).

The interferometer mirrors when hit by a cosmic ray undergo both excitation of the internal degree of freedom and of the suspension pendulum modes. The mirror's internal degrees of freedom are excited both by the heat produced with an amplitude given by eq. (13.1), and by the differential momentum released by the cosmic rays. The excitation of the mirror pendulum mode by cosmic muons has been evaluated by Weiss [1972] considering only ionization losses.

In a subsequent work of Amaldi and Pizzella [1986] the effect of production of knock-on electrons, bremsstrahlung, direct pair production and photonuclear interactions by muons was shown to be crucial for the evaluation of the cosmic muon noise in a bar antenna. A Monte Carlo simulation of the background due to high-energy cosmic muons in a bar antenna has been done by Ricci [1987].

A calculation taking into account both ionization losses and the four processes mentioned for an antenna having 3 km arm length and 400 kg quartz mirror mass, has been done by Giazotto [1988b]. The results show that muons of 10^2 GeV give 1 ms pulses having $h \simeq 10^{-23}$ with a frequency of 10^2 yr^{-1} and 10^4 GeV muons give $h \simeq 10^{-21}$ with a frequency of 10^{-6} yr^{-1}.

For periodic GW the calculation gives the following measurability condition for $\tilde{h}$:

$$\tilde{h} > 10^{-25} / \nu^2 \ \mathrm{Hz}^{-1/2} \ , \tag{13.2}$$

where the GW frequency ν has been assumed to be larger than the pendulum frequency and smaller than the frequency of the lowest mode of the mirror.

14. Conclusions

In this section the relevant types of noise described previously, limiting the interferometer's sensitivity, are evaluated as a function of the GW frequency and compared with the GW strain amplitude of some astrophysical sources. For the evaluation of these types of noise the following parameters characterizing the interferometer are assumed: arm length $L = 3$ km, FP finesse $F = 40$, suspension quality factor $Q = 10^6$, mirror quality factor $Q_1 = 10^5$, temperature $T = 300$ K, frequency and mass of the lowest longitudinal mode of the mirror $\nu_1 = 2500$ Hz and $M_1 = 150$ kg, respectively, mirror mass $M = 300$ kg, vacuum pipe pressure $P = 10^{-7}$ mb assuming the residual gas to be H_2, recirculated light power $W = 1$ kW and seismic noise spectral displacement $x_T \cong 3 \times 10^{-7} / \nu^2$ m$\sqrt{\mathrm{Hz}}$.

In fig. 14.1 the interferometer sensitivity is shown as a function of the characteristic frequency of the incident GW, which is assumed to be the inverse of the pulse duration of the GW, together with some relevant types of noise and astrophysical GW source amplitudes. Line a is the sensitivity limit due to seismic noise reaching the mirrors suspended as a simple 1 m pendulum, line b represents the limit due
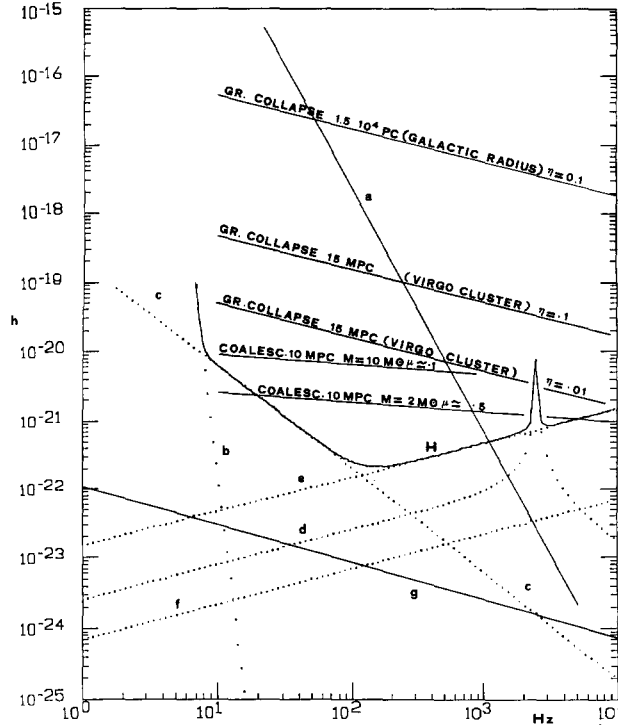
Fig. 14.1. The sensitivity to an incident GW of a 3 km arm length interferometer, whose physical parameters are defined in the text; the observation frequency is assumed to be the inverse of the GW pulse duration. The types of noise are: a, seismic noise (1 m simple pendulum), b, seismic noise [Del Fabbro et al. 1988b], c, mirror suspension thermal noise, d, mirror first longitudinal mode thermal noise, e, photon counting noise, f, pressure fluctuations in the vacuum pipe (FP), g, quantum limit. H is the resulting interferometer sensitivity assuming the seismic noise to be given by curve b. The expected amplitudes for gravitational collapse [see eq. (I.2)] in the Galaxy ($\eta = 0.1$) and in the Virgo cluster ($\eta = 0.1, 0.01$) are also shown; the amplitudes for coalescing binaries have been evaluated for ($M = 2\,M_\odot$, $\mu = 0.5$) and ($M = 10\,M_\odot$, $\mu \approx 0.1$), integrating over the time given by eq. (I.4).
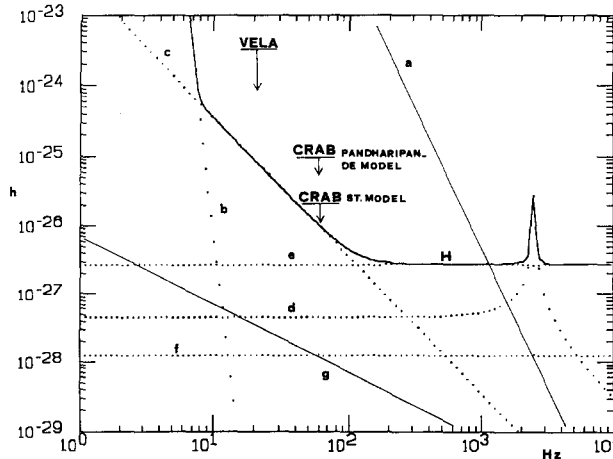
Fig. 14.2. The sensitivity of a 3 km arm length interferometer, whose physical parameters are defined in the text, to periodical GW, assuming a 1 yr integration time. The symbols are explained in the caption to fig. 14.1. The upper limits to the GW amplitudes of the Vela and Crab pulsars [Zimmermann 1978, Pandharipande et al. 1976] are expected to be in the sensitivity range of the interferometer (curve H) if seismic noise is assumed to be given by curve b.

to seismic noise filtered by the attenuator described by Del Fabbro et al. [1988b], line c represents the suspension thermal noise and line d the mirror's first longitudinal normal mode thermal noise, line e represents photon counting noise, line f represents the noise due to vacuum pipe gas fluctuations and line g the quantum limit.

The amplitudes of gravitational collapse have been evaluated using eq. (I.2) assuming the frequency to be the inverse of the collapse duration. The coalescence amplitudes have been evaluated using eq. (I.3) integrated over the time elapsed given by eq. (I.4). The total noise b + c + d + e + f + g is shown by the line H.

The interferometer sensitivity to periodic signals integrated over 1 year is shown in fig. 14.2; the noise symbols are the same as in fig. 14.1. The upper limits to the GW amplitudes emitted by the Vela and Crab pulsars are also shown.

Acknowledgements

References

Aguirregabiria, J.M. and L. Bel, 1987, Phys. Rev. A 36 3768.
Allega, A.M. and N. Cabibbo, 1983, Lett. Nuovo Cimento 38, 263.
Amaldi, E. and G. Pizzella, 1986, Nuovo Cimento 9C, 612.
Araki, H., J. Ehlers, K. Hepp, R. Kippenhahn, H.A. Weidenmüller and J. Zittartz, 1984, in: Gravitation, Geometry and Relativistic Physics, Proc.
    (Aussois, France, 1984), Lecture Notes in Physics, Vol. 212 (Springer, Berlin).
Barone, F., L. Milano, I. Pinto and G. Russo, 1988, Astron. Astrophys. 203, 322.
Bel, L., J-L. Boulanger and N. Deruelle, 1988, Phys. Rev. A 37, 1210.
Berger, J. and J. Levine, 1974, J. Geophys. Res. 79, 8.
Bernard, C., A. De Rújula and B. Lautrup, 1984, Nucl. Phys. B 242, 93.
Beron, B.L. and R. Hofstadter, 1969, Phys. Rev. Lett. 23, 184.
Billing, H., K. Maischberger, A. Rüdiger, R. Schilling, L. Schnupp and W. Winkler, 1979, J. Phys. E 12, 1043–1050.
Billing, H., W. Winkler, A. Rüdiger, R. Schilling, K. Maischberger and L. Schnupp, 1983, The Munich gravitational wave detector using laser
    interferometry, in: Quantum Optics, Experimental Gravity and Measurement Theory, eds P. Meyestre and M.O. Scully (Plenum, New York).
M. Born and E. Wolf, 1964, Principles of Optics (Pergamon, Oxford).
Bradaschia C., R. Del Fabbro, L. Di Fiore, A. Di Virgilio, A. Giazotto, H. Kautzky, V. Montelatici and D. Passuello, 1989, Phys. Lett. A 137, 329.
Braginskii, V.B. and A. Manoukine, 1974, Mesure de Petites Forces dans les Experiences Physiques (Mir, Moscow).
Braginskii, V.B. and M. Menskii, 1971, JEPT Lett. 13, 417.
Braginskii, V.B. and V.N. Rudenko, 1978, Phys. Rep. 46, 165.
Braginskii, B.V., L.P. Grishchuk, A.G. Doroshkevich Ya.B. Zel'Dovich, I.D. Novikov and M.V. Sazhin, 1974, Sov. Phys.–JETP 38, 865.
Braginskii, V.B., C.M. Caves and K.S. Thorne, 1977, Phys. Rev. D 15, 2047.
Brillet, A., 1984, The interferometric detection of gravitational waves, in: Gravitation, Geometry and Relativistic Physics, Proc. (Aussois, France,
    1984), Lecture Notes in Physics, Vol. 212 (Springer, Berlin).
Brillet, A., 1985, Ann. de Phys. 10, 219–226.
Campani, E., A. Giazotto and D. Passuello, 1986, Rev. Sci. Instrum. 57, 79.
Camy, G., D. Pinayd, N. Courtier and Hu Chi Chuan, 1982, Rev. Phys. Appl. 17, 357–363.
Caves, C.M., 1980, Phys. Rev. Lett. 45, 75.
Chandrasekhar, S., 1970, Phys. Rev. Lett. 24, 611.
Clark, J.P.A., E.P.J. van den Heuvel and W. Sutantyo, 1979, Astron. Astrophys. 72, 120.
Del Fabbro, R., A. Di Virgilio, A. Giazotto, H. Kautzky, V. Montelatici and D. Passuello, 1987, Phys. Lett. A 124, 253.

Del Fabbro, R., A. Di Virgilio, A. Giazotto, H. Kautzky, V. Montelatici and D. Passuello, 1988a, Rev. Sci. Instrum. 59, 292.

Del Fabbro, R., A. Di Virgilio, A. Giazotto, H. Kautzky, V. Montelatici and D. Passuello, 1988b, Phys. Lett. A 132, 237.

Del Fabbro, R., A. Di Virgilio, A. Giazotto, H. Kautzky, V. Montelatici and D. Passuello, 1988c, Phys. Lett. A 133, 471.

Deruelle, N. and P. Tourrenc, 1984, in: Gravitation, Geometry and Relativistic Physics, Proc. (Aussois, France, 1984), Lecture Notes in Physics, Vol. 212 (Springer, Berlin).

Diambrini Palazzi, G. and D. Fargion, 1987, Phys. Lett. B 197, 302.

Dorsel, A., J.D. McCullen, P. Meystre, E. Vignes and H. Walther, 1983, Phys. Rev. Lett. 51, 1550.

Douglass, H.D. and V.B. Braginskii, 1979, in: General Relativity (Cambridge Univ. Press, Cambridge).

Drever, R.W.P., 1981, Gravitational wave detectors using laser interferometers and optical cavities, 1. Ideas, principles and prospects, Invited lecture given at Nato Advanced Study Institute on Quantum Optics and General Relativity (Bad Windesheim, Germany).

Drever, R.W.P., 1982, Interferometric detectors for gravitational radiation, in: Gravitational Radiation, Proc. Les Houches Summer Institute, eds T. Piran and N. Deruelle.

Drever, R.W.P., G.M. Ford, J. Hough, I.M. Kerr, A.J. Munley, J.R. Pugh, N.A. Robertson and H. Ward, 1980, in: Proc. Ninth Intern. Conf. on General Relativity and Gravitation (Jena, 1980), ed. E. Schmutzer (Deutscher Verlag der Wissenschaften, Berlin).

Drever, R.W.P., J. Hough, A.J. Munley, S.A. Lee, R. Spero, S.E. Whitcomb, H. Ward, G.M. Ford, M. Hereld, N.A. Robertson, I. Kerr, J.R. Pugh, G.P. Newton, B. Meers, E.D. Brooks III and Y. Gursel, 1981, Optical cavity laser interferometers for gravitational wave detection, in: Laser Spectroscopy V, eds A.R.W. McKellar, T. Oka and B.P. Stoicheff (Springer, Berlin).

Drever, R.W.P., J.L. Hall, F.V. Kowalski, J. Hough, G.M. Ford, A.J. Munley and H. Ward, 1983, Appl. Phys. B 31, 97–105.

Edelstein, W.A., J. Hough, J.R. Pugh and W. Martin, 1978, J. Phys. E 11, 710.

Einstein, A., 1916, Preuss. Akad. Wiss. Berlin, Sitzungsber. Phys. Math. Kl., 688.

Faller, J.E. and R.L. Rinker, 1979, Super Spring, Dimensions, September, p. 25.

Faller, J.E., P.L. Bender and R.T. Stebbins, 1987, The development of very low frequency isolation systems for ground-based gravitational wave interferometers, NSF Grant No. Phy-87 12072.

Fattaccioli, D., A. Boulharts, A. Brillet and C.N. Man, 1986, J. Opt. (Paris) 17, No. 3, 115–128.

Forward, R.L., 1978, Phys. Rev. D 17 379.

Forward, R.L., 1979, J. Appl. Phys. 50, No. 1, 1–6.

Friedman, J.L. and B.F. Schutz, 1978, Astrophys. J. 222, 345.

Gea-Banacloche, J. and G. Leuchs, 1987, J. Mod. Optics 34, 793.

Gersenshtein, M.E. and V.I. Pustovoit, 1963, Sov. Phys. – JETP 16, 433.

Giazotto, A., 1987, The seismic noise challenge to the detection of low frequency gravitational waves, in: 7th Congr. of General Relativity and Gravitational Physics (Rapallo, Italy, 1986) (World Scientific, Singapore) p. 449.

Giazotto, A., 1988a, The VIRGO project: a wide band antenna for gravitational wave detection, in: Proc. VIII Convegno Nazionale di Relatività Generale e Fisica della Gravitazione (Cavalese).

Giazotto, A., 1988b, Phys. Lett. A 128, 241.

Giazotto, A., E. Campani, D. Passuello and A. Stefanini, 1986a, Performance of an active pendulum with interferometric sensing, in: Proc. Fourth Marcel Grossman Meeting on the Recent Developments of General Relativity (Rome, 1985), ed. R. Ruffini (Elsevier Sci. Publ., Amsterdam).

Giazotto, A., D. Passuello and A. Stefanini, 1986b, Rev. Sci. Instrum. 57, 1145.

Gold, T., 1968, Nature 218, 731.

Goorvitch, D., 1975, Appl. Opt. 14, 1387–1390.

Grassi Strini, A.M., G. Strini and G. Tagliaferri, 1980, J. Appl. Phys. 51, 849.

Hall, J.L., H.P. Layer and R.D. Deslattes, 1977, IEEE J. Quantum Electron. QE-13, 45–46D.

Hernandez, G., 1986, Fabry Pérot Interferometer (Cambridge Univ. Press, Cambridge).

Herriott, D., H. Kogelnik and R. Kompfner, 1964, Appl. Opt. 3, 523–526.

Hough, J., 1987, Report on round table discussion – gravitational wave detectors, in: Proc. NATO Advanced Research Workshop on Gravitational Wave Data Analysis (Cardiff, 1987).

Hough, J., R.W.P. Drever, A.J. Munley, S.-A. Lee, R. Spero, S.E. Whitcomb, H. Ward, G.M. Ford, M. Hereld, N.A. Robertson, I. Kerr, J.R. Pugh, G.P. Newton, B. Meers, E.D. Brooks III, Y. Gursel, 1983, Gravitational wave detectors using laser interferometers and optical cavities: some practical aspects and results, in: Quantum Optics, Experimental Gravity and Measurement Theory, eds P. Meyestre and M.O. Scully (Plenum, New York).

Hough, J., D. Hils, M.D. Rayman, L.-S. Ma, L. Hollberg and J.L. Hall, 1984, Appl. Phys. B 33, 179–185.

Hough, J., B.J. Meers, G.P. Newton, N.A. Robertson, H. Ward, B.F. Schutz, R.W.P. Drever, R. Mason, C. Pollard, R. Tolcher, D.W. Bellenger, J.R.J. Bernnett, I.F. Corbett and M.D. Percival, 1986, A British long baseline gravitational wave observatory, GWD/RAL/86-001.

Hough, J., B.J. Meers, H.P. Newton, N.A. Robertson, H. Ward, B.F. Schutz, I.F. Corbett and R.W.P. Drever, 1987, Vistas Astron. 30, 109–134.

Kerr, G.A., N.A. Robertson, J. Hough and C.N. Man, 1985, Appl. Phys. B 37, 11–16.

Kojima, Y. and T. Nakamusa, 1984, Prosp. Theor. Phys. 71, 79.

Kuroda, K., K. Tsubono and H. Hirakawa, 1982, Phys. Lett. 92A, 131.

Landau, L. and E. Lifshitz, 1951, The Classical Theory of Fields (Pergamon, New York).

Leuchs, G., K. Maischberger, A. Rüdiger, R. Schilling, L. Schnupp and W. Winkler, 1987, Proposal for the construction of a large laser interferometer for the measurement of gravitational waves, MPQ 129 and MPQ 131.

Linet, B. and P. Tourrenc, 1976, Can. J. Phys. 34, 1129–1133.

Linsay, P. and D. Shoemaker, 1982, Rev. Sci. Instrum. 53, 1014.

Livas, J., R. Benford, D. Dewey, A. Jeffries, P. Linsay, P. Saulson, D. Shoemaker and R. Weiss, 1986, The MIT prototype gravitational wave detector, in: Proc. Fourth Marcel Grossmann Meeting on the Recent Developments of General Relativity (Rome, 1985), ed. R. Ruffini (Elsevier Sci. Publ., Amsterdam).

Lorenzini, D.A., 1972, Active control of a pneumatic isolation system, in: Proc. AIAA Guidance and Control Conf. (Stanford, CA, 1972), Paper No. 72-843.

Lyne, A.G., R.N. Manchester and H.J. Taylor, 1985, Mon. Not. R. Astron. Soc. 213, 613.

Maischberger, K., A. Rüdiger, R. Schilling, L. Schnupp, W. Winkler and H. Billing, 1979, Noise investigation in a laser interferometer for the detection of gravitational radiation, presented by A. Rüdiger at Second Marcel Grossmann Meeting on the Recent Developments of General Relativity (Trieste, Italy, 1979).

Man, C.N., 1988, External modulation and recyclings, at: European Collaboration Meeting on Interferometric Detection of GW (Sorrento, 1988).

Man, C.N., A. Brillet and D.S. Shoemaker, 1986, at: European Collaboration Meeting on Large Interferometers (Chantilly, 1986).

Man, C.N., A. Brillet and D.S. Shoemaker, 1987, Gravitational wave data analysis, at: Nato Workshop (Cardiff, 1987).

Manchester, R.N. and J.H. Taylor, 1981, Astron. J. 86, 1953.

Meers, B.J., 1983, Opt. Commun. 47, 237.

Meers, B.J., 1988, Phys. Rev. D 38, 2317.

Meystre, P., E.M. Wright, J.D. McCullen and E. Vignes, 1985, J. Opt. Soc. Am. B 2, 1830.

Misner, C.W., K.S. Thorne and J. Wheeler, 1973, Gravitation (Freeman, San Francisco) (cited in the text as MTW).

Newton, G.P., J. Hough, G.A. Kerr, B.J. Meers, N.A. Robertson, H. Ward, J.B. Mangan, S. Hoggan and R.W.P. Drever, 1986, Some improvements to the Glasgow gravitational wave detector, in: Proc. Fourth Marcel Grossmann Meeting on the Recent Developments of General Relativity (Rome, 1985), ed. R. Ruffini (Elsevier Sci. Publ., Amsterdam).

Pacini, F., 1968, Nature 219, 145.

Pandharipande, V.R., D. Pines and R.A. Smith, 1976, Astrophys. J. 208, 550.

Paris, Orsay, Pisa, Napoli, Frascati Collab., 1988, VIRGO project: a progress report, presented to Fifth Marcel Grossmann Meeting (Perth, Australia, 1988), INFN PI/AE 88/10.

Pegoraro, F., E. Picasso and L.A. Radicati, 1978, J. Phys. A 11, 1949.

Pisa, Napoli, Frascati, Orsay, Paris Collab., 1987, VIRGO project, INFN PI/AE 87/1.

Pizzella, G., 1975, Riv. Nuovo Cimento 5, No. 3.

Rawley, L.A., J.H. Taylor and M.M. Davis, 1986, Nature 319, 383.

Ricci, F., 1987, Nucl. Instrum. Methods Phys. Res. A 260, 491–500.

Robertson, N.A., R.W.P. Drever, I. Kerr and J. Hough, 1982, J. Phys. E 15, 1101–1105.

Rüdiger, A., 1988, private communication.

Rüdiger, A., R. Schilling, L. Schnupp, W. Winkler, H. Billing and K. Maischberger, 1981a, Opt. Acta 28, 641–658.

Rüdiger, A., R. Schilling, L. Schnupp, W. Winkler, H. Billing and K. Maischberger, 1981b, J. de Phys. 42, C8-451.

Rüdiger, A., R. Schilling, L. Schnupp, D. Shoemaker, W. Winkler, G. Leuchs and K. Maischberger, 1987, The Garching 30-meter prototype and plans for a large gravitational wave detector, in: Proc. 18th Texas Symp. on Relativistic Astrophysics (Chicago 1986), ed. M.P. Ulmer (World Scientific, Singapore).

Ruggiero, F., 1979, Alcuni problemi relativi alla rivelazione delle onde gravitazionali, Thesis, Pisa Univ., unpublished.

Saulson, P.R., 1984a, Phys. Rev. D 30, 732.

Saulson, P.R., 1984b, Rev. Sci. Instrum. 55, 1315.

Schilling, R., L. Schnupp, W. Winkler, H. Billing, K. Maischberger and A. Rüdiger, 1981, J. Phys. E 14, 65.

Schilling, R., L. Schnupp, D.H. Shoemaker, W. Winkler, H. Billing, K. Maischberger and A. Rüdiger, 1984, Improved sensitivities in laser interferometers for the detection of gravitational waves, in: Gravitation, Geometry and Relativistic Physics, Proc. (Aussois, France, 1984), Lecture Notes in Physics, Vol. 212 (Springer, Berlin).

Schnupp, L., W. Winkler, K. Maischberger, A. Rüdiger and R. Schilling, 1985, J. Phys. E 18, 482.

Shoemaker, D., 1987, Contributions à l'etude de la detection interferometrique des ondes de gravitation, Thesis, Univ. Paris XI.

Shoemaker, D., W. Winkler, K. Maischberger, A. Rüdiger, R. Schilling and L. Schnupp, 1985, Progress with the Garching 30-meter prototype for a gravitational wave detector, MPQ 100.

Shoemaker, D., R. Schilling, L. Schnupp, W. Winkler, K. Maischberger and A. Rüdiger, 1987a, Noise behavior of the Garching 30 meter prototype gravitational wave detector, MPQ 130.

Shoemaker, D.S., A. Brillet and C.N. Man, 1987b, Wide bandwidth frequency and power stabilization of a laser-diode-pumped Nd:YAG laser, in: Proc. Conf. on Lasers and Electro-Optics, Vol. 14 (Opt. Soc. Am.).

Shoemaker, D.S., A. Brillet, C.N. Man, O. Crégut and G. Kerr, 1989, A frequency-stabilized laser-diode pumped Nd:YAG laser, Opt. Lett., in press.

Spero, R., 1986, The Caltech laser-interferometric gravitational wave detector, in: Proc. Fourth Marcel Grossmann Meeting on the Recent Developments of General Relativity (Rome, 1985), ed. R. Ruffini (Elsevier Sci. Publ., Amsterdam).

Taylor, J.H. and R.N. Manchester, 1977, Astrophys. J. 215, 885.

Thorne, K.S., 1980, Rev. Mod. Phys. 52, 285.

Thorne, K.S., 1987, in: Three Hundred Years of Gravitation (Cambridge Univ. Press, Cambridge).

Thorne, K.S., 1989, Light Scattering and Proposed Baffle Configuration for the LIGO-GRP 200 (Caltech).

Tourrenc, P. and N. Deruelle, 1985, Ann. de Phys. 10, 241–252.

Uhlenbeck, G.E. and L.S. Ornstein, 1930, Phys. Rev. 36, 823.

Vinet, J-Y., 1981, Nuovo Cimento 64A, 163.

Vinet, J-Y., 1986, J. de Phys. 47, 639–643.

Vinet, J-Y., B. Meers, C.N. Man and A. Brillet, 1988, Phys. Rev. D 38, 433–447.

Wagoner, R.V., 1984, Astrophys. J. 278, 345.

Ward, H., J. Hough, G.A. Kerr, N.L. Mackenzie, J.B. Mangan, B.J. Meers, G.P. Newton, D.I. Robertson and N.A. Robertson, 1987, The Glasgow gravitational wave detector – present progress and future plans, in: Proc. Intern. Symp. on Experimental Gravitational Physics (Guangzhou, China, 1987).

Weiss, R., 1972, Quart. Progr. Rep. Res. Lab. Electron. MIT 105, 54.

Weiss, R., 1979, in: Sources of Gravitational Radiation, ed. L.L. Smarr (Cambridge Univ. Press, Cambridge).

Winker, W., 1977, Experimental gravitation (Atti dei Convegni Lincei).

Zimmermann, M., 1978, Nature 271, 525.

Zimmermann, M., 1980, Phys. Rev. D 21, 891.

Zimmermann, M. and E. Szedenits Jr, 1979, Phys. Rev. D 20, 351.